Journal of Applied Sciences

ISSN 1812-5654

science alert

ANSInet
an open access publisher
http://ansinet.com

Journal of Applied Sciences 13 (24): 5766-5795, 2013
ISSN 1812-5654 / DOI: 10.3923/jas.2013.5766.5795

Numerical Research on Aerodynamic Performance of a Van

[1]Zheng Wei, [1]Qian-Jian Guo and [2]Xiao-Ni Qi
[1]School of Mechanical Engineering,
[2]School of Transportation and Vehicle Engineering, Shandong University of Technology,
Private bag, Zibo, 255049, China

Abstract: This study studies the van of 118 made in chang'an company and the modified models. According to the simulation, the aerodynamic characteristics of the small van and the modified vans are obtained. The conclusion is that the drag of modified small vans are lower than the initial one by analyzing the aerodynamic performance of small vans. The computed results can give a reference for study of the aerodynamic resistance reduction on a van for energy saving. And the results of the optimized shape can provide a theoretical basis for the related research.

Key words: Van, numerical simulation, aerodynamic resistance

INTRODUCTION

Vans play an important role among commercial vehicles. Fifty to seventy percent of the van's power (70-100 km h^{-1} speed) is consumed in overcoming aerodynamic resistance. A simple analysis of this data set suggests that even 1% reduction in the aerodynamic drag can amount to a significant saving in the fuel cost (Kassim and Filippone, 2010; Ferrai, 2009). New technologies have greatly increased the practical vehicle speed, so the aerodynamic resistance increases highly. As the driving velocity increases, the aerodynamic resistance that is in direct proportion to the square of the velocity and the fuel consumption increases correspondingly.

Although, the study of energy saving for the conveyance is focused on cars and passenger cars (Hemida and Baker, 2010; Cogotti, 2008; Yao *et al*., 2010; Nasir *et al*., 2012; Watkins and Gioacchino, 2008; Khaled *et al*., 2012; Regert and Lajos, 2007; Kieffer *et al*., 2006; Gohlke *et al*., 2010), some achievements have been obtained in experimental research on the energy saving technology of a van recently. But the numerical research is just beginning and starts to attract more attention (Al-Garni and Bernal, 2010; Huang *et al*., 2010; Rahman and Ikeura, 2012; Shuk *et al*., 2012; Ni *et al*., 2010; Wang *et al*., 2010; Li *et al*., 2010).

This study studies the 3-D numerical calculation on the flow field of a van. The RNG k-ε turbulence models and the momentum method are used to calculate the 3-D flow fields and the coefficient of resistance, respectively. In addition, the mechanism of the decrease in resistance by changing the van configuration is obtained. The results can supply a necessary reference for a van design.

NOMENCLATURE

A	=	Sectional area in cross-direction of flowing fluid (m^2)
B	=	Width of truck (m)
b_{fv}	=	Length of vertical bar in the fence (m)
b_{fh}	=	Length of horizontal bar in the fence (m)
C_d	=	Coefficient of resistance
$C_{1\varepsilon}$	=	Constant in production term of e-equation
$C_{2\varepsilon}$	=	Constant in dissipation term of k-equation
C_μ	=	Experimental constant in turbulent viscosity equation
D	=	Gap between drive cab and container (mm)
F_d	=	Aerodynamic resistance (N)
F_f	=	Surface friction (N)
F_p	=	Pressure drag Fp (N)
F_q	=	Rate of change of momentum (N)
H	=	Height of truck (mm)
h_f	=	Height of fence (m)
k	=	Turbulent kinetic energy (m^2s^{-2})
L	=	Total length of truck (mm)
l	=	Length of computational domain (m)
P	=	Relative pressure (Pa)
p	=	Pressure (Pa)
R	=	Additional source term

Corresponding Author: Xiao-Ni Qi, School of Transportation and Vehicle Engineering, Shandong University of Technology, Zibo, China

μ = Laminar viscosity (kg $m^{-1}s^{-1}$)
U_1 = Air velocity postulated (ms^{-1})
x = Coordinates (m)
x_f = Abscissa of the fence (m)
y_f = Ordinate of the fence (m)
α_k = Turbulent Prandtl number for k
α_e = Turbulent Prandtl number for e
β = Constant in RNG k-e models
δ_{ij} = Kronecker delta function
ε = Rate of turbulence energy dissipation (m^2s^{-3})
η = Ratio of turbulent to mean strain time scale
η_0 = Constant in strain dependent term
S_{ij} = Magnitude of strain rate (s^{-1})
μ_t = Turbulent dynamic viscosity (kg m^{-1} s^{-1})
μ_{eff} = Effective viscosity (kg m^{-1} s^{-1})
ρ = Density (kg m^{-3})
$\bar{\tau}_{ij}$ = Stress tensor (kg m^{-1} s^{-2})
i,j, k = Index variable of Cartesian components

MATERIALS AND METHODS

Numerical simulation

Assumptions and physical model: The van studied in this study is 118 style van made in Chang'an Company, the length, the width and the height of which is 11270×2490×3520 mm, respectively. The simplified van model, head modified, tail modified and roof modified models are shown in Fig. 1.

Considering the demands for computational accuracy, we make the following assumptions on the van:

The air is an incompressible fluid.

The influence of smaller appended devices, such as the rearview mirror, the doorknob is neglected and the smaller radian of the bodywork surface is neglected.

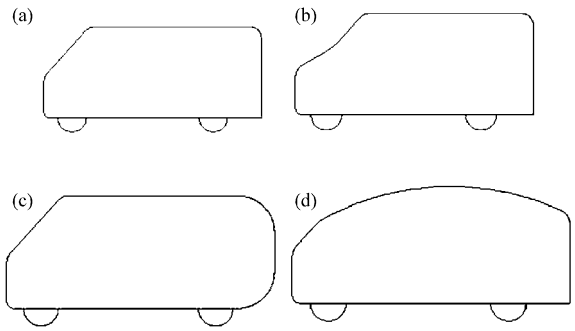

Fig. 1(a-d): Diagram of original model and modified models (a) 118 style mode, (b) Head modified model, (c) Tail modified model and (d) Roof modified model

The temperature, reference pressure and viscosity of the air are constant, the parameters under the condition of this study are listed in Table 1 and the airflow around a van is stead.

Mathematical model: The RNG k-ε turbulence models are used to simulate the flow field around the van. This model is more suitable to calculate a separated flow field. It is different from the standard k-ε turbulence model only in terms of the coefficients and the source (Tsubokura *et al*., 2010; Hyams *et al*., 2011). The air flowing around the van can be considered as a steady turbulent fluid flow. So the control differential equations and the model equations can be described as follows (Yakhot and Orszag, 1986).

For a 3-D incompressible fluid, the Reynolds averaged control equations can be expressed in the general cartesian tensor form as:

- Mass continuity equation:

$$\frac{\partial \bar{u}_i}{\partial x_i} = 0 \tag{1}$$

- Momentum equation:

$$\frac{\partial}{\partial x_j}(\rho \bar{u}_i \bar{u}_j - \bar{\tau}_{ij}) = -\frac{\partial \bar{p}}{\partial x_i} \tag{2}$$

- Stress equation:

$$\bar{\tau}_{ij} = 2\mu S_{ij} - \frac{2}{3}\mu_t \frac{\partial \bar{u}_k}{\partial x_k}\delta_{ij} \tag{3}$$

- Turbulent viscosity:

$$\mu_t = \frac{\rho C_\mu k^2}{\varepsilon} \tag{4}$$

where, ρ, $\bar{u}$, p, μ, μ_t, k, ε and $\bar{\tau}$ are the density, velocity, pressure, viscosity, turbulent viscosity, turbulent kinetic energy, turbulence energy dissipation rate and stress tensor, respectively. The variables designated by the superscript "-" are time averaged values. The distortion rate tensor S_{ij} and the Kronecker delta function δ_{ij} can be written as:

Table 1: Parameters under the numerical condition

Temperature (°C)	Pressure (Pa)	Viscosity (Pa sec)	Density (kg m^{-3})
25	1.0135×10^5	1.5021×10^{-5}	1.205

$$S_{ij} = \frac{1}{2}\left(\frac{\partial \bar{u}_i}{\partial x_j} + \frac{\partial \bar{u}_j}{\partial x_i}\right) \text{ and } \delta_{ij} = \begin{cases} 0, & i \neq j \\ 1, & i \neq j \end{cases}$$

Reynolds averaged turbulent kinetic energy equation:

$$\frac{\partial(\rho \bar{u}_i k)}{\partial x_j} = \frac{\partial}{\partial x_j}\left(\alpha_k \mu_{eff} \frac{\partial k}{\partial x_j}\right) + \mu_t S^2 - \rho\varepsilon \quad (5)$$

where, the effective viscosity μ_{eff} and the mean rate of strain tensor variable S are defined as $\mu_{eff} = \mu+\mu_t$ and $S=\sqrt{2S_{ij}S_{ij}}$, respectively.

Reynolds averaged turbulence energy dissipation rate equation:

$$\frac{\partial(\rho \bar{u}_i \varepsilon)}{\partial x_i} = \frac{\partial}{\partial x_i}(\alpha_\varepsilon \mu_{eff} \frac{\partial \varepsilon}{\partial x_i}) + C_{1\varepsilon}\mu_t S^2 \frac{\varepsilon}{k} - C_{2\varepsilon}\rho\frac{\varepsilon^2}{k} - R \quad (6)$$

where, R is the additional source which is the main difference between the RNG k-ε turbulence models and the standard k-ε turbulence models. It takes the following form:

$$R = \frac{C_\mu \rho \eta^3 (1-\eta/\eta_0)}{1+\beta\eta^3}\frac{\varepsilon^2}{k} \quad (7)$$

where, $\eta = Sk/\varepsilon, \eta_o = 4.38, \beta = 0.012.$ Equation 5 represents the relationship between the additional source and the stream distortion rate. The additional source term R becomes significant for flows with large strain rates, i.e., when $\eta >> \eta_0$. The parameter η is a measure of the ratio of the turbulent to mean time scale. In the field of weak strain where S and η tend to zero, the additional source term tends to zero and the standard form of the k-ε models is restored. In the limit of strong strain where S and η tend to infinity, the additional source term R becomes:

$$R = \frac{\rho C_\mu \eta \varepsilon^2}{\beta \eta_0 k}$$

where, η_0 is the fixed point for homogeneously strained turbulent flows and β is a constant evaluated to yield a von Karman constant of about 0.41. The strain in the separated flow of a van lies between these two limits. The values of other experimental constants in above Eq. can be taken as (Yakhot and Orszag, 1986):

$$\alpha_k = \alpha_\varepsilon = 1.393, C_{1\varepsilon} = 1.42\ ,\ C_{2\varepsilon} = 1.68,\ C_\mu = 0.0845$$

Grids in computational domain: In addition to the physical model and the selected computational domain, the quality of the computational grids also has crucial influence on the calculation accuracy. Bad grids even cause the evaluation not to converge, not to mention the CPU time. A fixed 3-D Cartesian coordinate system is used in the computational domain. According to the research of Kobayashi (Toshio and Kozo, 1992), the trail region and the top region should not be smaller than five times and two times the width of the model, respectively. Thus the flow field around the model may not be influenced by the boundary. So the computational domain should not be smaller but a larger domain would increase the quantity of calculation greatly. In this computation, the computational domain is 18 B long, 5 B wide and 3.5 H high, where B and H are the width and height of the van, respectively. Finer grids are employed in regions where the flow changes tempestuously to increase the computational accuracy and coarser grids are used where the flow changes mildly to reduce CPU time. Figure 2 shows the grids in the computational domain.

Boundary conditions: Since, the numerical calculation cases are for a steady state, the solution of the fluid differential equations requires boundary conditions but not initial conditions. The boundary conditions must be mathematically consistent, so the solution of the differential equations can be existent and unique. There are several boundary conditions in the flow field around the van: Inlet, outlet, walls and computational domain profiles. When a van is running, there is no boundary layer on the ground. In the wind tunnel experiments, the ground boundary layer must be eliminated but the ground boundary cannot be removed because the van model must be laid on a flat plate that simulates the ground in the experiment. A similar fixed floor is adopted in the calculation in order to compare the results with those obtained from the experiment easily. According to the actual flow field around the van, the boundary conditions can be specified as follows:

- **Inlet:** u = U1, v = w = 0, p = p1, where U1 is the air velocity in the distance. U1 = 20 m sec^{-1} (30 m sec^{-1}) in the computation
- **Outlet:** u = U1, v = w = 0, p = p1, the influence of the outlet section on the computational domain
- **Walls:** In the computational domain, wall boundaries, including the ground and the surface of the van, are all non-slip boundaries, at which u = v = w = 0

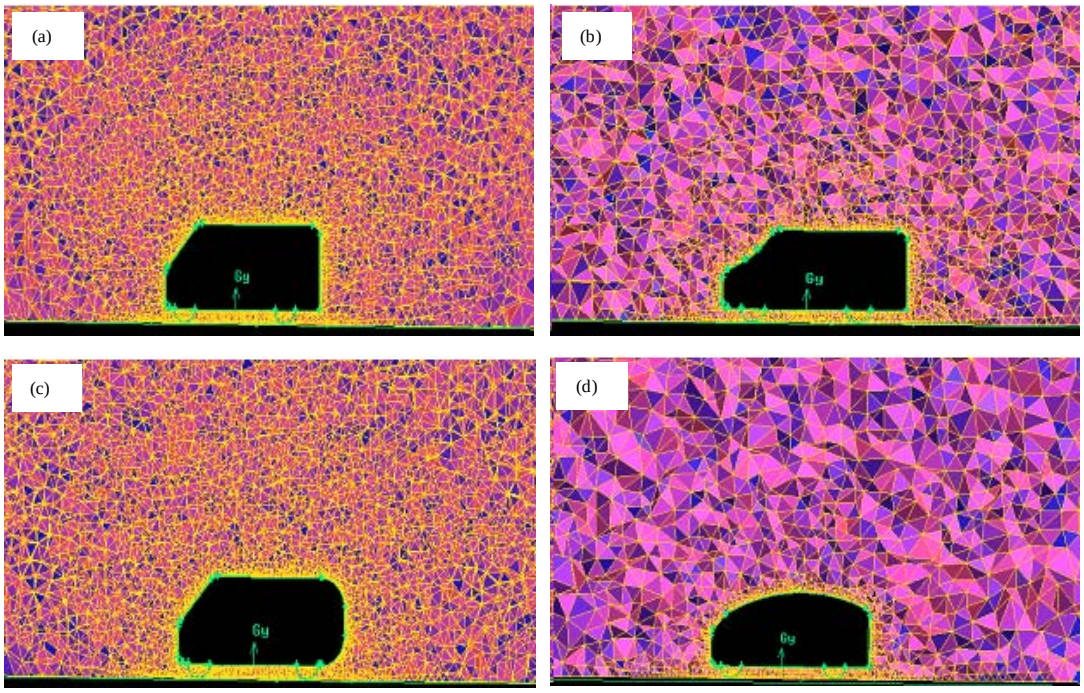

Fig. 2(a-d): Sketch of the computational domain (a) 118 style mode, (b) Head modified model, (c) Tail modified model and (d) Roof modified model

- **Upside and profiles:** the computational domain on the upside and the profiles of the van are wide enough and high enough that the influence of these boundaries can be neglected, so u = U1, v = w = 0, p = p1

Numerical methods: In this article, all conservation equations and turbulence model equations are solved using the CFD software FLUENT, based on the finite-volume method. The first-order upwind different method is adopted for convective terms and the central differencing for diffusive terma. To evaluate the pressure-velocity coupling field, the well-known SIMPLE algorithm is employed.

RESULTS AND DISCUSSION

As the van has a larger frontal area and the clearance of the vehicle body with the ground is relatively larger, there are flow separation field around the top, the bottom and the left and right sides. The large rear area of will result in a larger wake in the rear area. In the wake zone, there are two types of spirals: Two horseshoe vortices (vertical vortices) and two symmetrical drag vortices (developed from two symmetric vortex on the cross section). In this study the aerodynamic characteristics of the original van were compared with those of the head-modified, tail-modified, roof-modified Vans. The vortex flow separation of the tail and the wake vortices were focused on to analyze the formation mechanism of the aerodynamic drag and lift which provides a theoretical basis on the optimization design of the aerodynamic shape.

Numerical results of A-style and B-style Vans

Analysis of pressure distribution: From Fig. 3 and 4 it was shown that the overall pressure distribution is as follows: The positive pressure zone forms in the area of the windscreens and the safety bar, other regions are negative pressure zone. The roof, bottom and the transition zone of the side and the head of the van formed a larger value of negative pressure zone; but the negative value is greater than that of the top area which is the formation mechanism of the lift. The transition zone of the top and the rear part also froms larger values of negative pressure zone. Under the both actions of the positive pressure in the head and the negative pressure in the tail, the pressure drag forms.

From the above analysis, a conclusion can be drawn that: By changing the shape of the head of the van, the pressure distribution on the van has little effect and thus the pressure drag on the van is not significantly affected.

Analysis on velocity distribution: From the flow field map in Fig. 5-8, the flow characteristics of the van can be obtained. The flow characteristic features are shown in

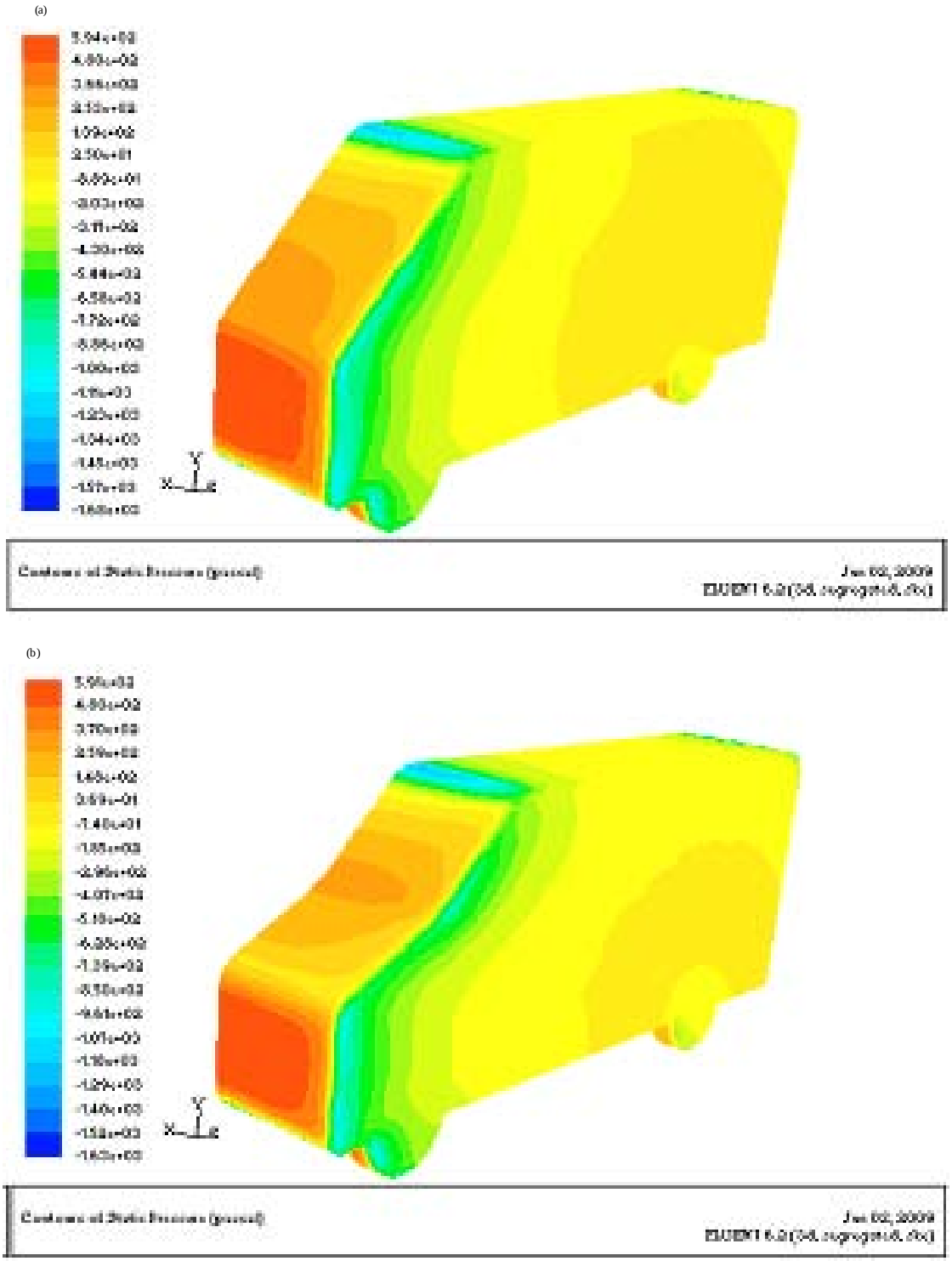

Fig. 3(a-b): Pressure distribution on van body surface

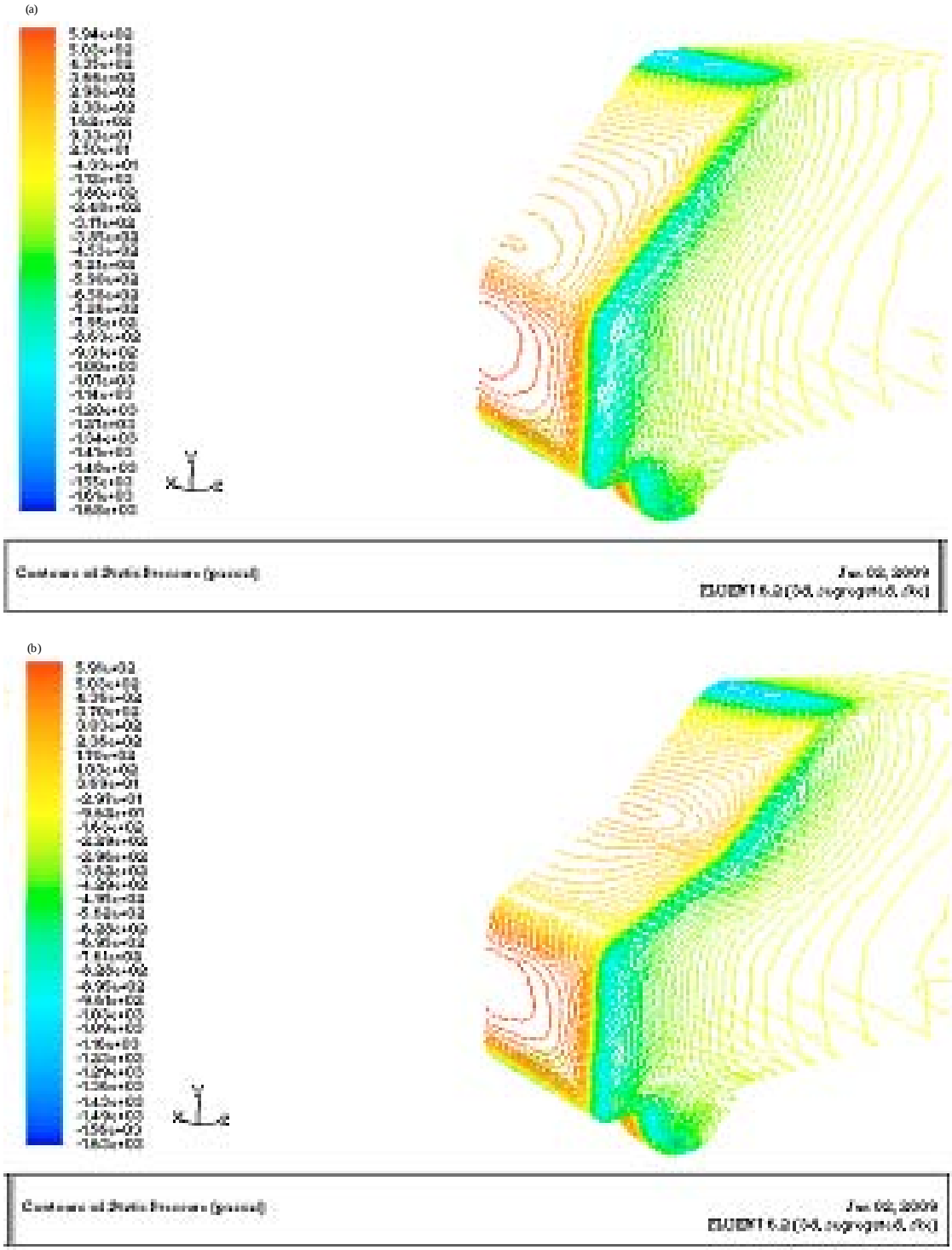

Fig. 4(a-b): Isobar distribution on van head

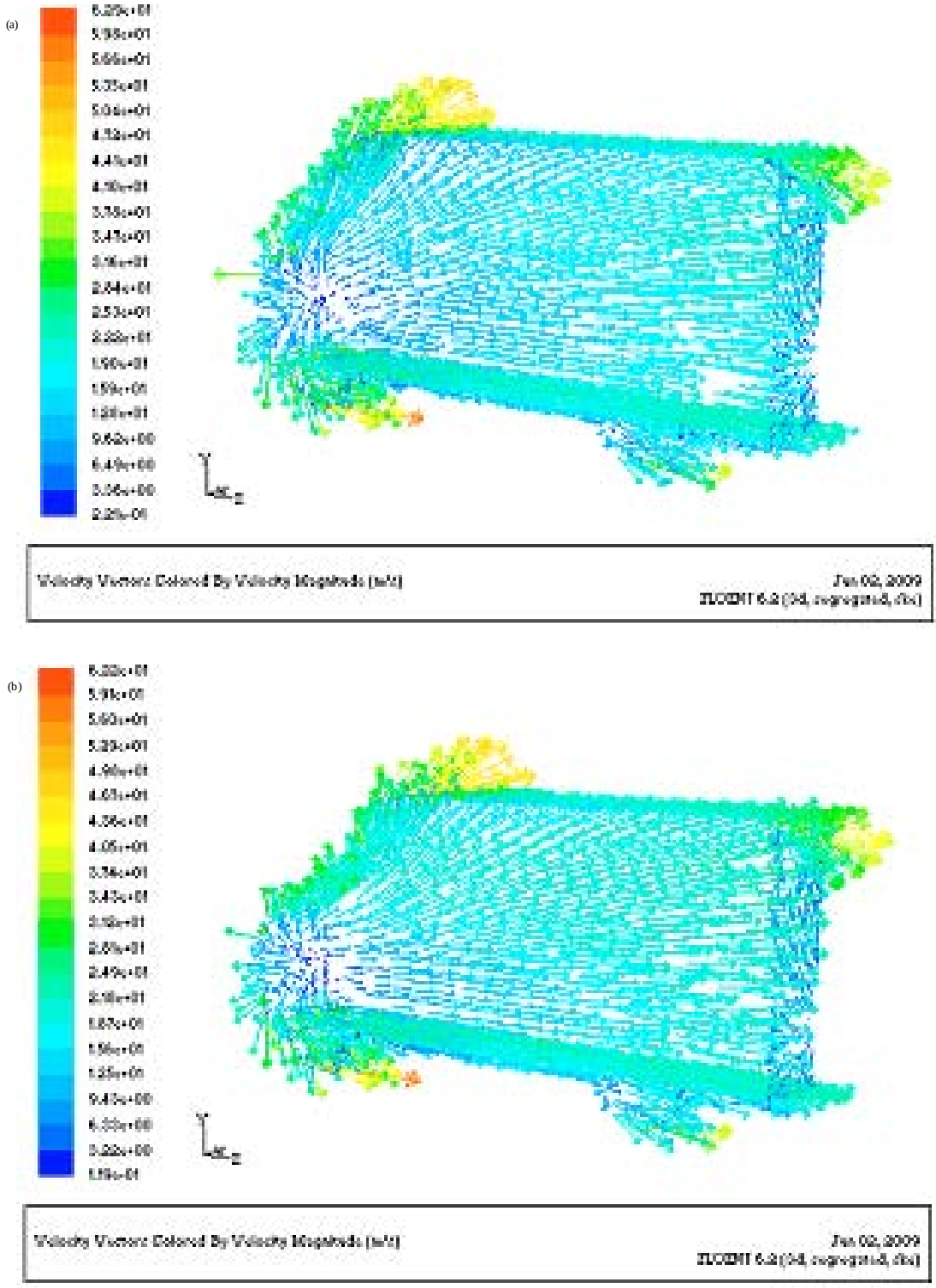

Fig. 5(a-b): Velocity vector on van body surface

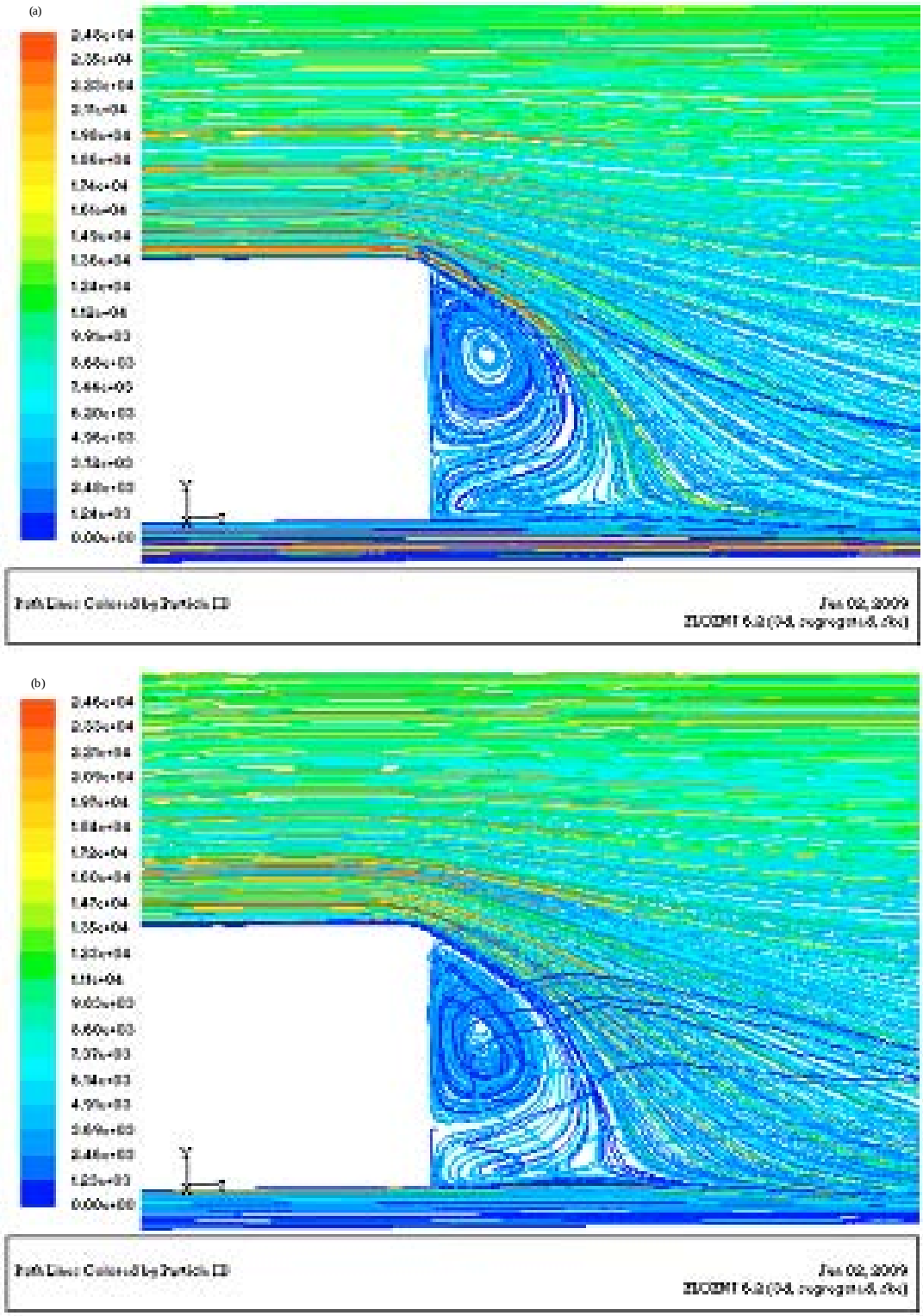

Fig. 6(a-b): Flow chart on symmetry plane

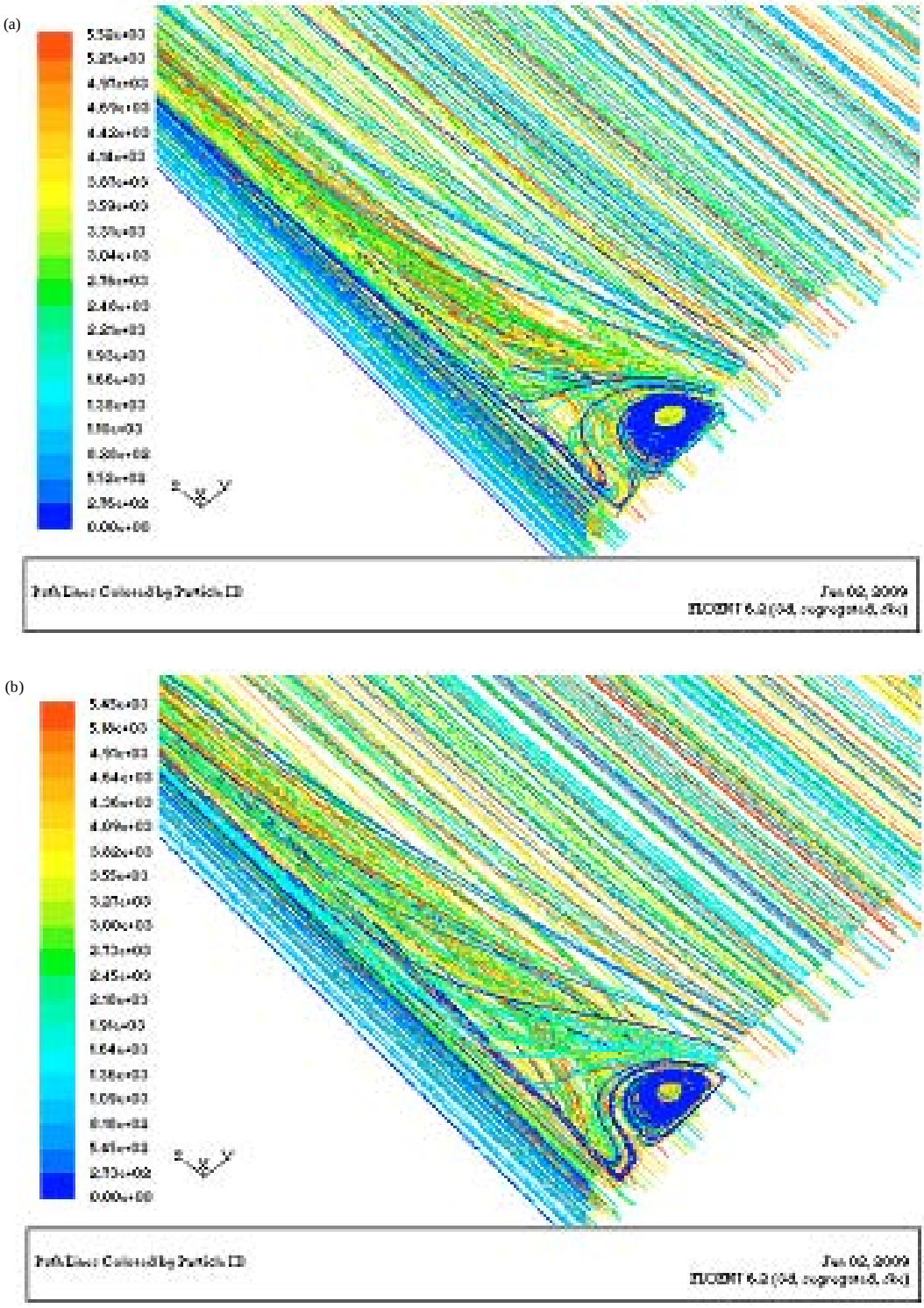

Fig. 7(a-b): Vortex distribution at Z = 230 mm

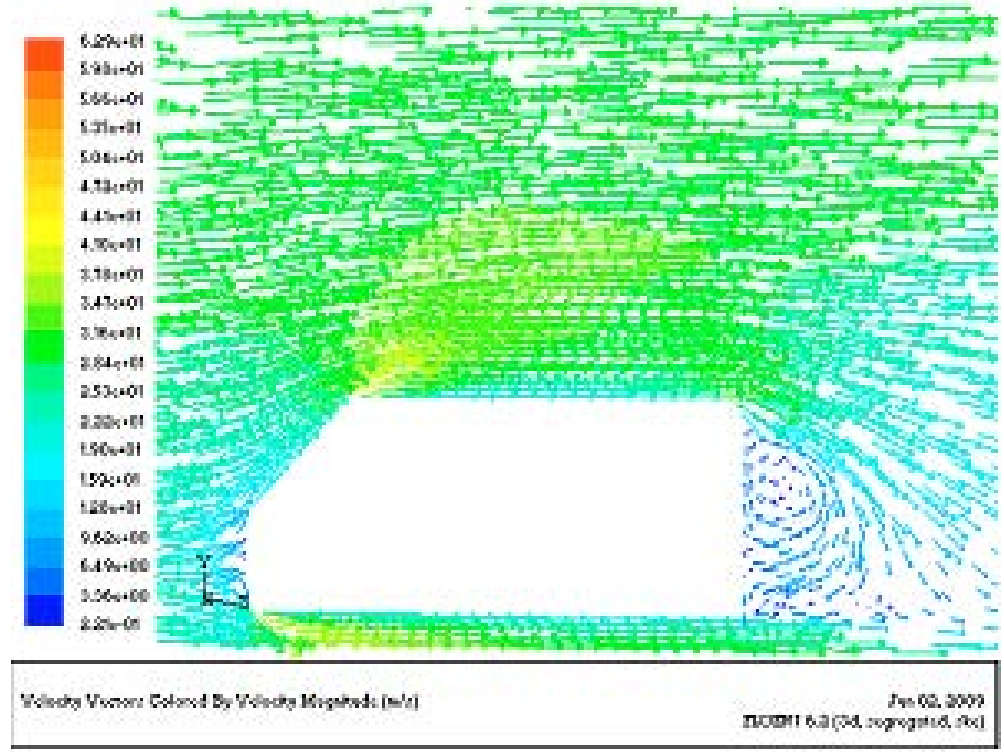

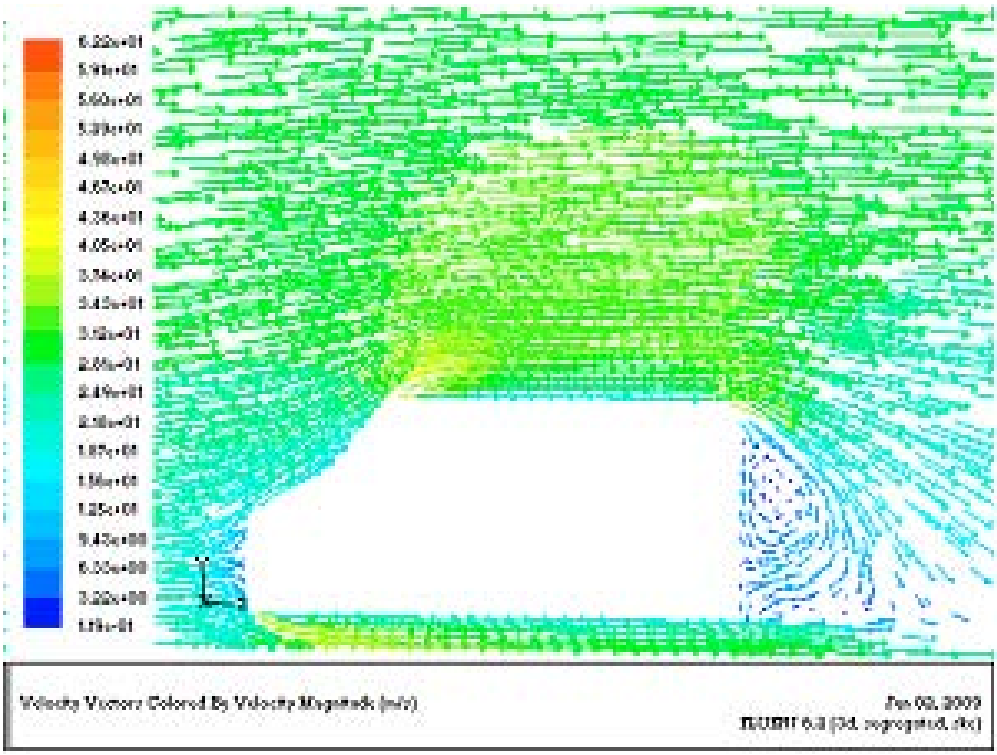

Fig. 8(a-b): Velocity vector in symmetry plane

Fig. 5 and 6: The airflow is blocked at the front safety bar and the air stagnation point is formed which results in the positive pressure areas. Then, the air flows into two parts, the upward airflow formed the negative pressure area on the crest of the cab and the bottom airflow is separated at the bottom edge. The top and bottom airflow roll up and down respectively which forms two longitudinal eddy current (as shown in Fig. 8, a large clockwise vortex in the upper part and a small counter-clockwise vortex in the lower part). These vortexes form the rear negative pressure area. At the same time the airflow separate on both sides of the van at the trailing edge which forms two symmetrical vortexes eventually developing into two symmetrical vortex drags. The four tail vortex is the root cause of the pressure drag.

From the above figures, flow line distribution on the upper body is more intensive and the velocity is relatively larger, especially there is a maximum value in the two corner on the roof. Moreover, the air is forced through the space between the van and the ground where the velocity of the air is larger. The airflow is obstructed at the junction of the hood and windshield where the air velocity is lower. In the wake region it is obvious to note that the minimum flow rate is 0~9 m sec^{-1} which shows the rear of the vehicle is most likely to form soil and dust adhesion.

It can be seen from Fig. 6 and 8 that the rear vortex of model A is slightly larger than that of model B which caused the resistance of A is larger. This is because model B the double dip transition in the front improves the aerodynamic characteristics of the van.

However, the drag reduction effect by means of the dual-angle windscreen is not very satisfactory. This is because that the nature of pressure drag is from the viscosity. To reduce the pressure drag, the positive pressure area in the van's front and the negative pressure area should mainly be reduced. How to reduce the positive pressure zone of the front of the van? The main method is to minimize the height and the front of the van as much as possible as well streamlined design. But for the van, the lower body height and streamlined design of the front of the van would greatly reduces the cargo volume which does not meet the design and use of personnel's mind. Therefore, reducing the negative pressure zone to reduce the tail pressure drag should be the main starting point of the van shape optimization.

Numerical results of A-style and C-style vans

Analysis of pressure distribution: The pressure distribution of model A has been analyzed in the above, the pressure distribution of model C will be analyzed in this section. The pressure distribution in the front part of model C and model A are similar but there is a big difference in the rear parts (as shown in Fig. 9~11). In modeling terms, the rear of model A is a common flat tail, the rear of model C is not the same, using the approximately arc type. because of the differences in shapes, there is a big difference in the rear pressure distribution. Compared with model A, the rear pressure rises more obviously. Based on the above formation mechanism of pressure drag and the shape features of model C, the resistance of model C is much smaller than that of model A. So that the purpose of drag reduction is achieved.

Analysis on velocity distribution: The velocity distribution of model A has been analyzed in the above, the velocity distribution of model C will be analyzed in this section. From Fig. 12~16, it was shown that the airflow separation of model C is different from that of model A. There is no symmetrical vortex in the rear symmetrical cross-section, the horseshoe vortex basically disappeared. Figure 16 shows that the drag vortex in the cross section of model C disappeared, either. This is because that the rear part of model C adopts the approximately arc transition, so top, the flow separation in the bottom and both sides of model C is smaller than those of model A and B and the vortex formation is more difficult. Furthermore, the rear arc transition can minimize the negative pressure area of the tail, so that the pressure drag will be greatly reduced.

Numerical results of A-style and D-style vans

Analysis of pressure distribution: The pressure distribution of model D will be analyzed in this section. It can be clearly seen from Fig. 17 and 18 that the positive pressure zone in the head decreases and the negative pressure in the tail zone reduces significantly. In the shape modeling aspects, modle D utilized the more common arch top. It was shown from Fig. 19 and 20 that the pressure gradient around the van body decreases. In general, the aerodynamic drag of model D is smaller than that of model A. However, the van's interior space is greatly reduced due to the use of arched roof which is inconsistent with the original intention of van users.

Analysis of velocity distribution: The velocity distribution and related aerodynamic characteristics of model D will be analyzed in this section. It was noted from Fig. 21~24 that the airflow separation of model D is different from that of model A. There is little symmetrical vortex in the rear symmetrical cross-section and the horseshoe vortex decreases greatly. Figure 25 shows that the drag vortex in the cross section of model D disappeared, either.

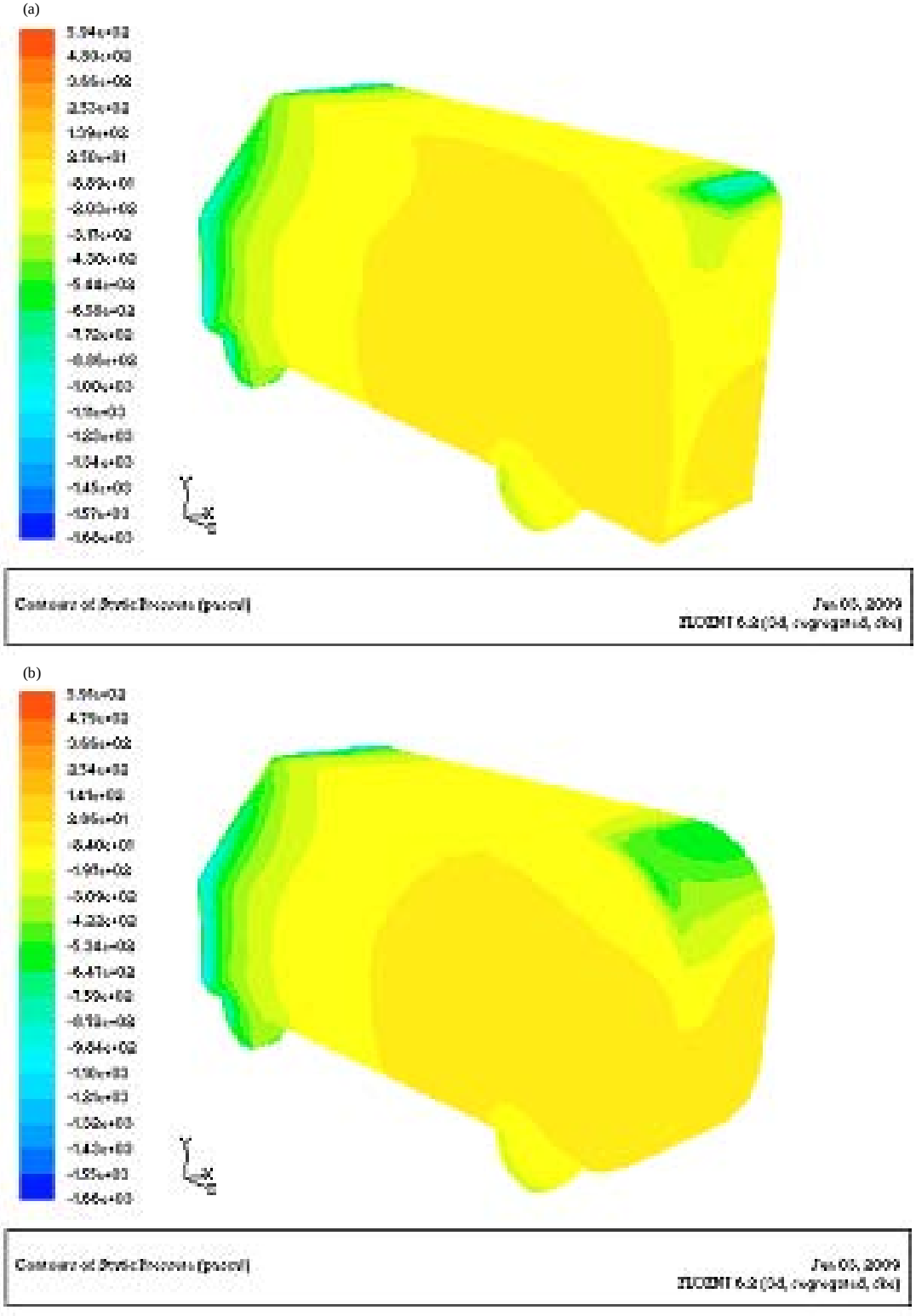

Fig. 9(a-b): Pressure distribution at tail

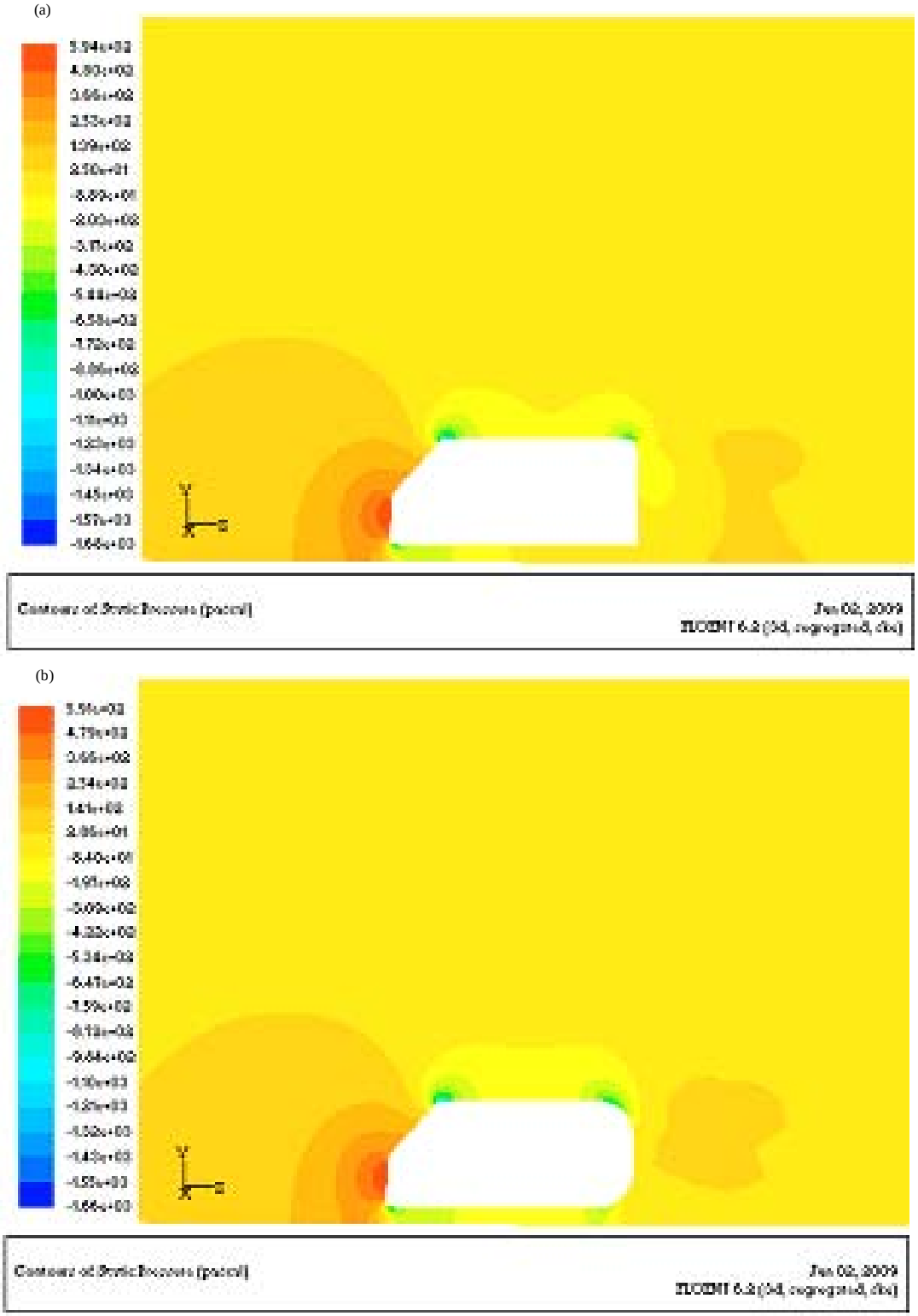

Fig. 10(a-b): Pressure distribution on symmetrical plane

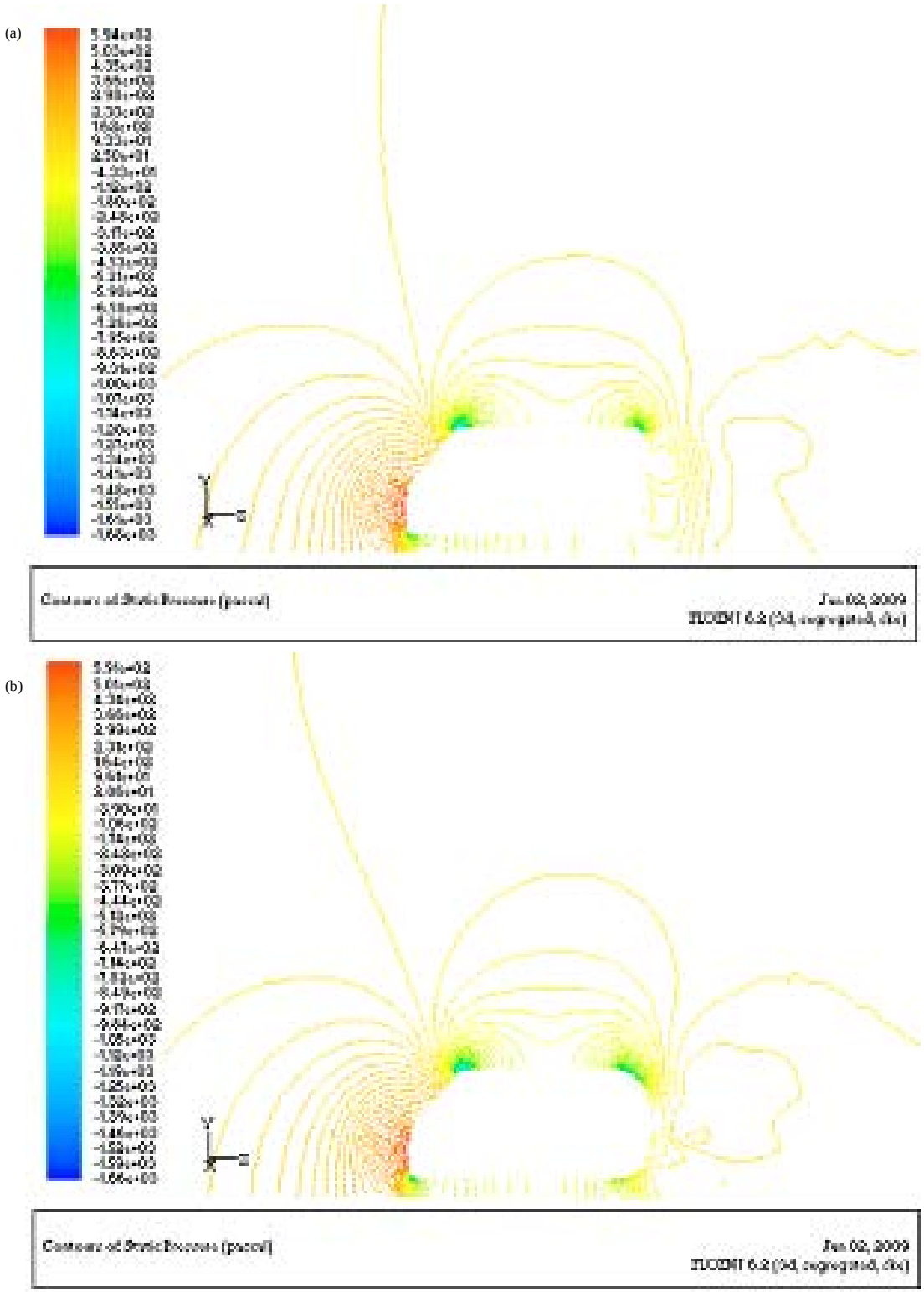

Fig. 11(a-b): Isobar distribution on symmetrical plane

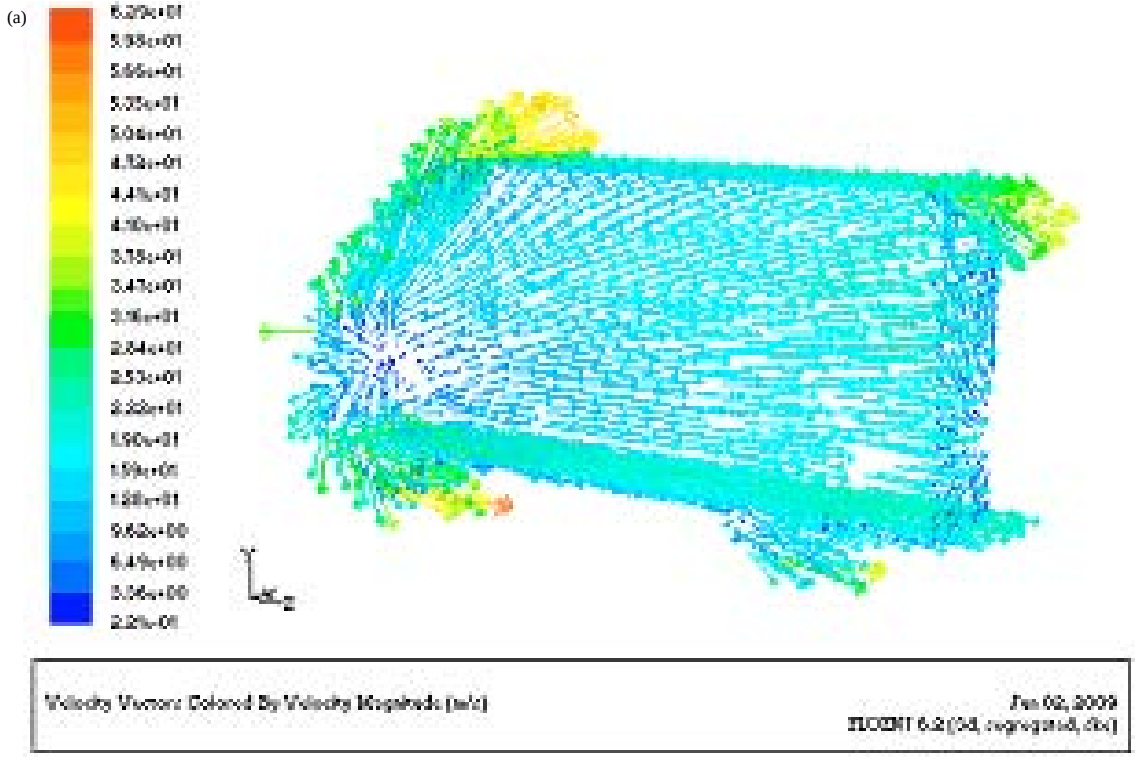

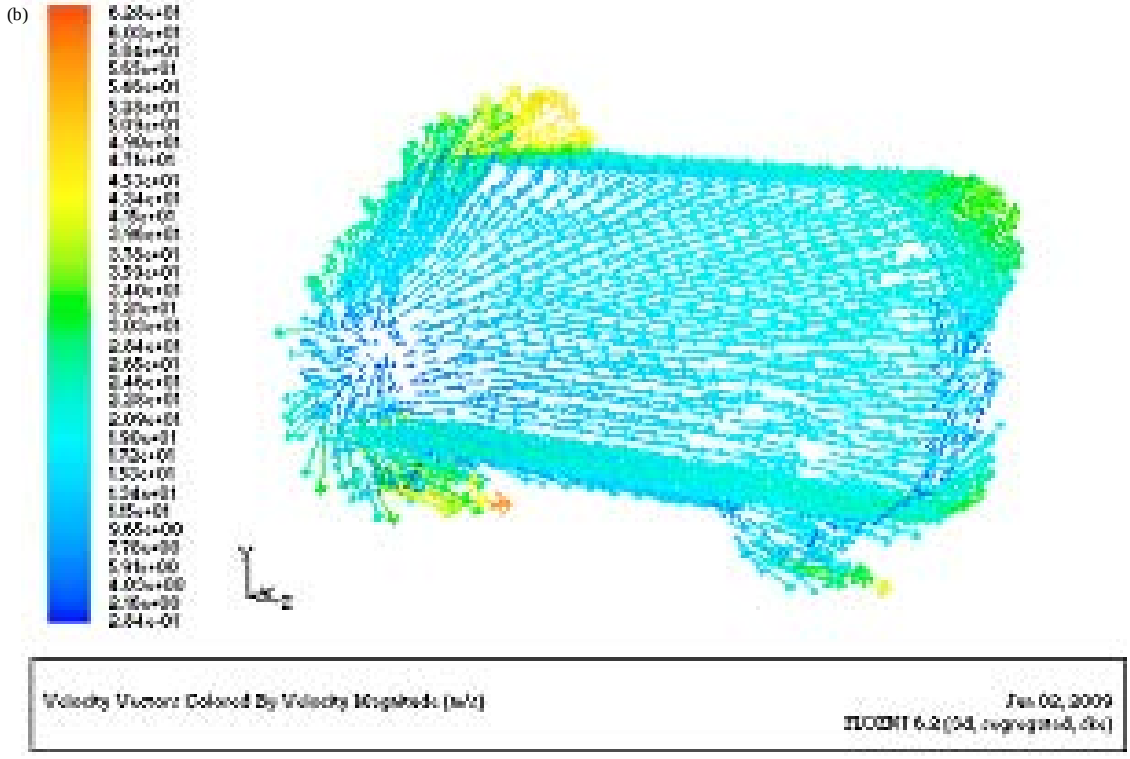

Fig. 12(a-b): Velocity vector on van body surface

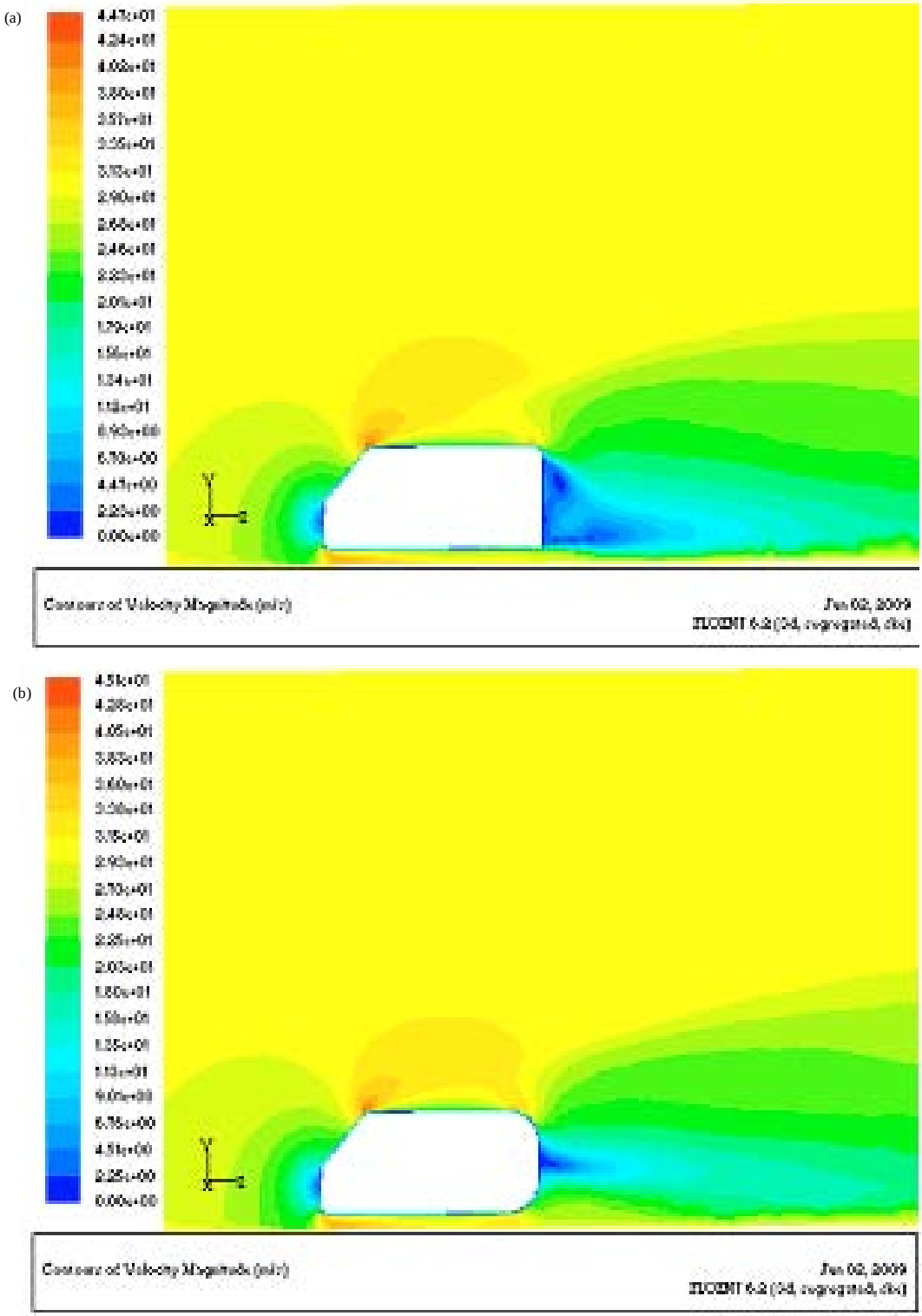

Fig. 13(a-b): Velocity distribution on symmetry plane

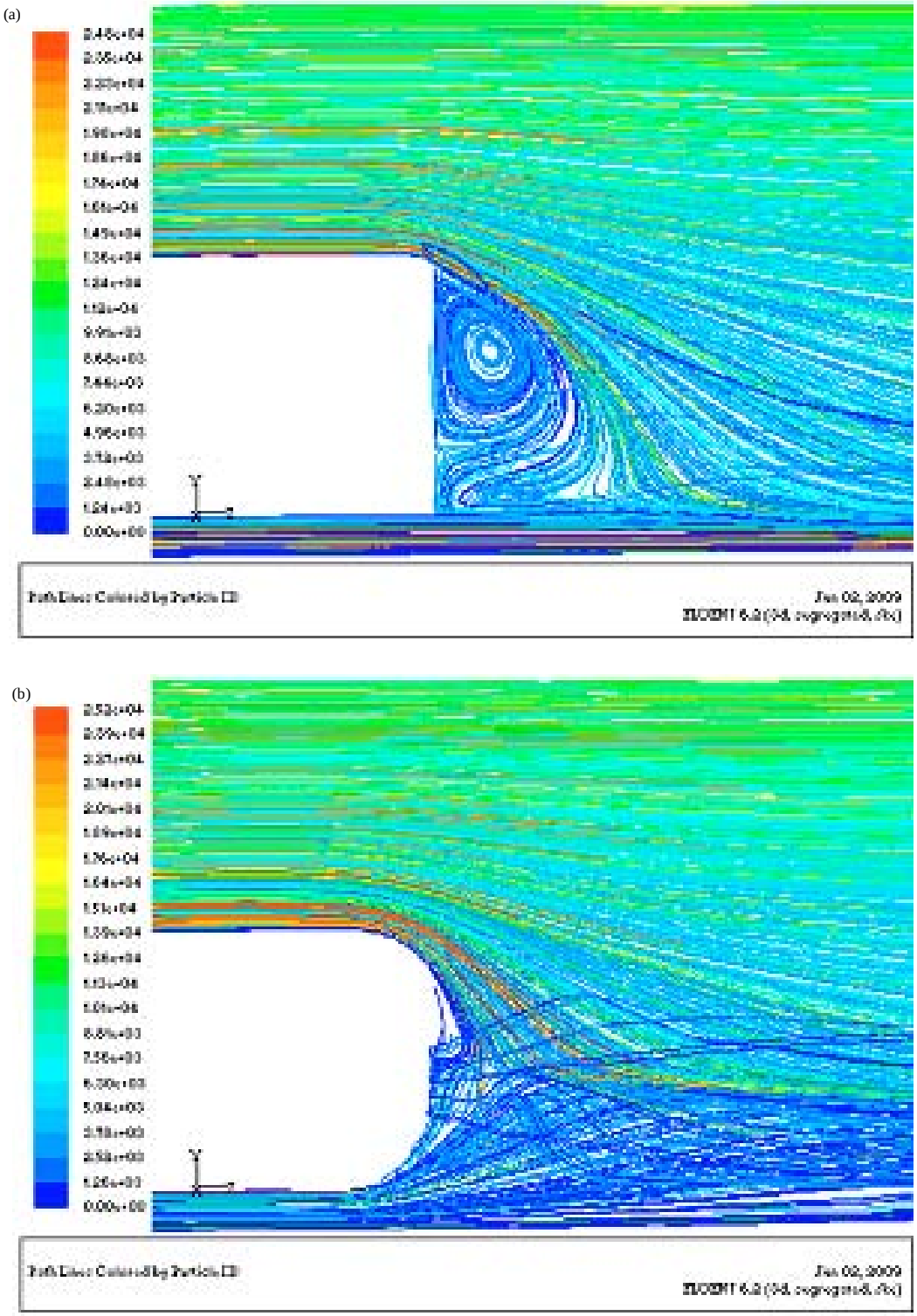

Fig. 14(a-b): Flow chart on symmetry plane

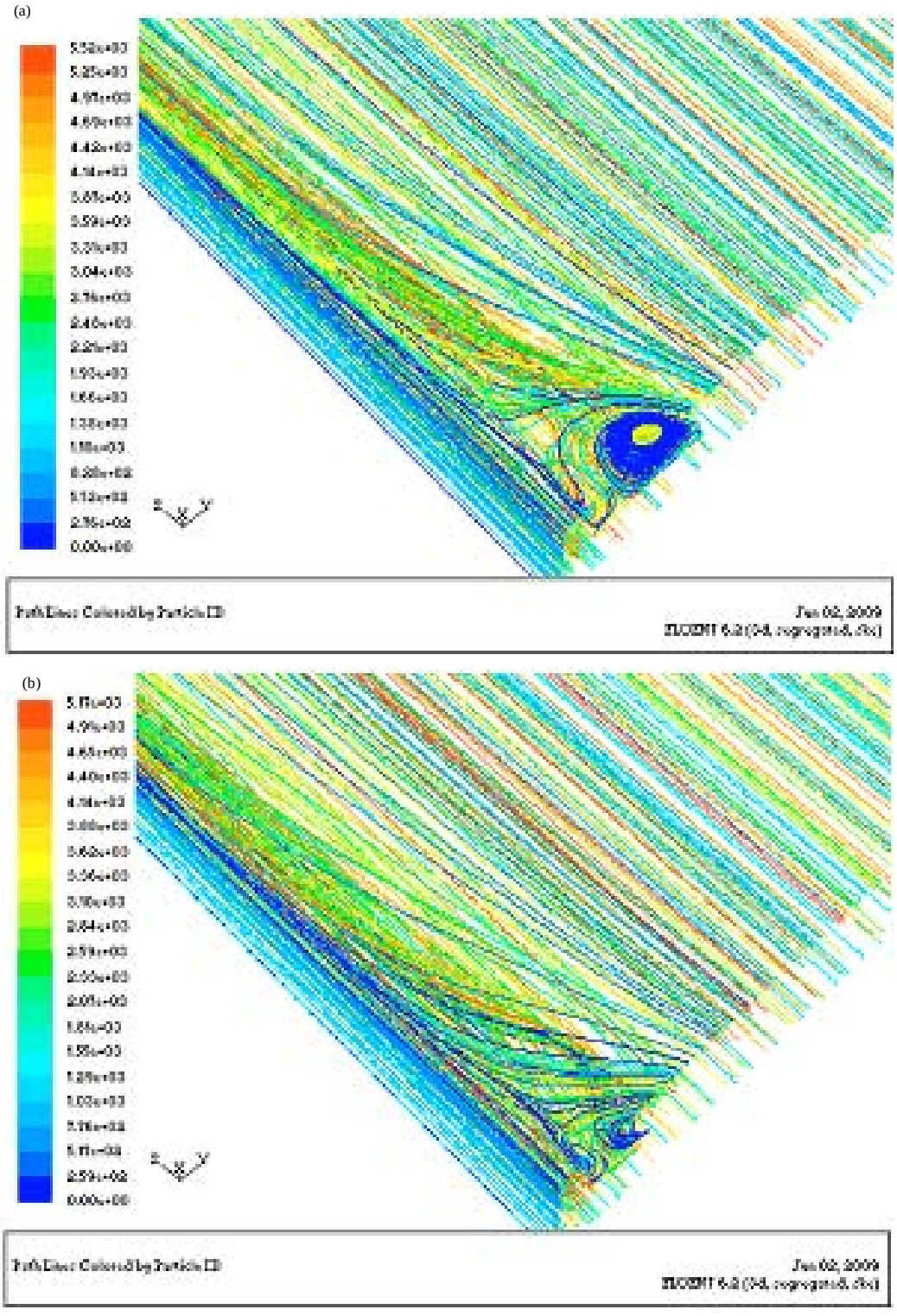

Fig. 15(a-b): Vortex distribution at Z = 230 mm

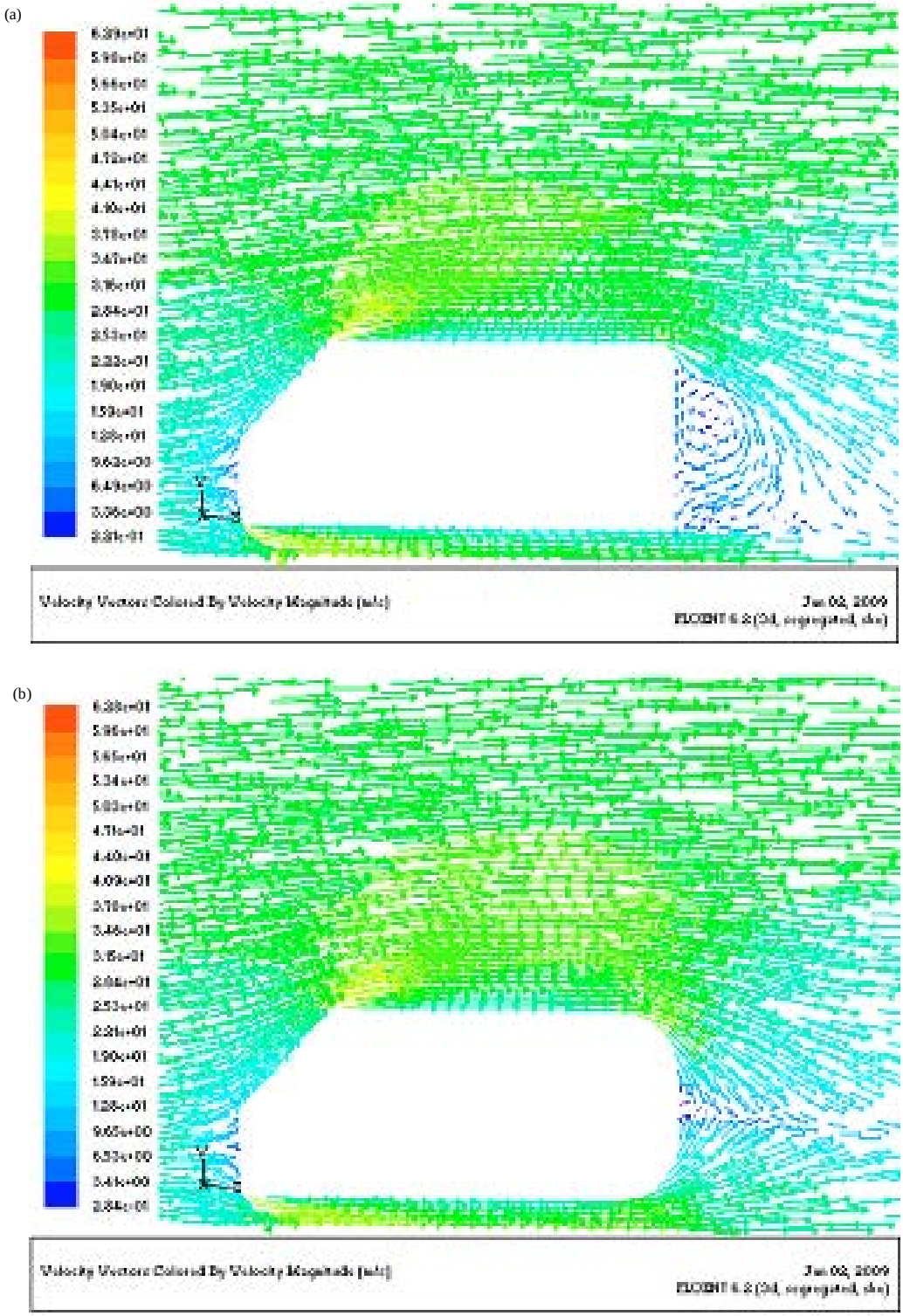

Fig. 16(a-b): Velocity vector in symmetry plane

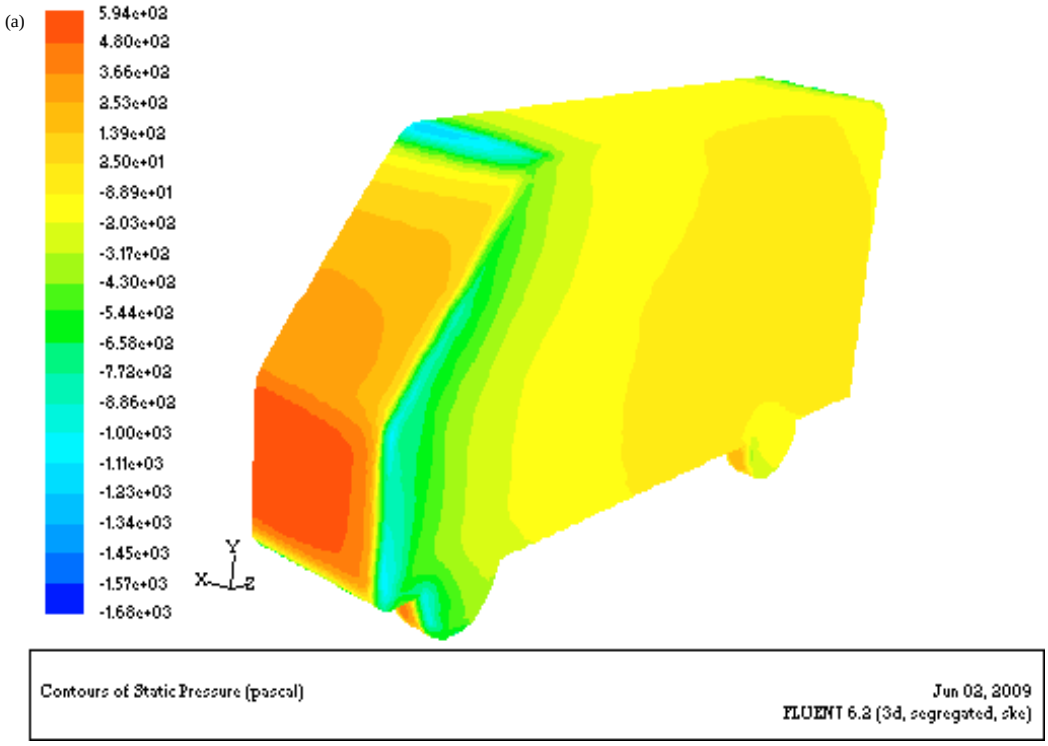

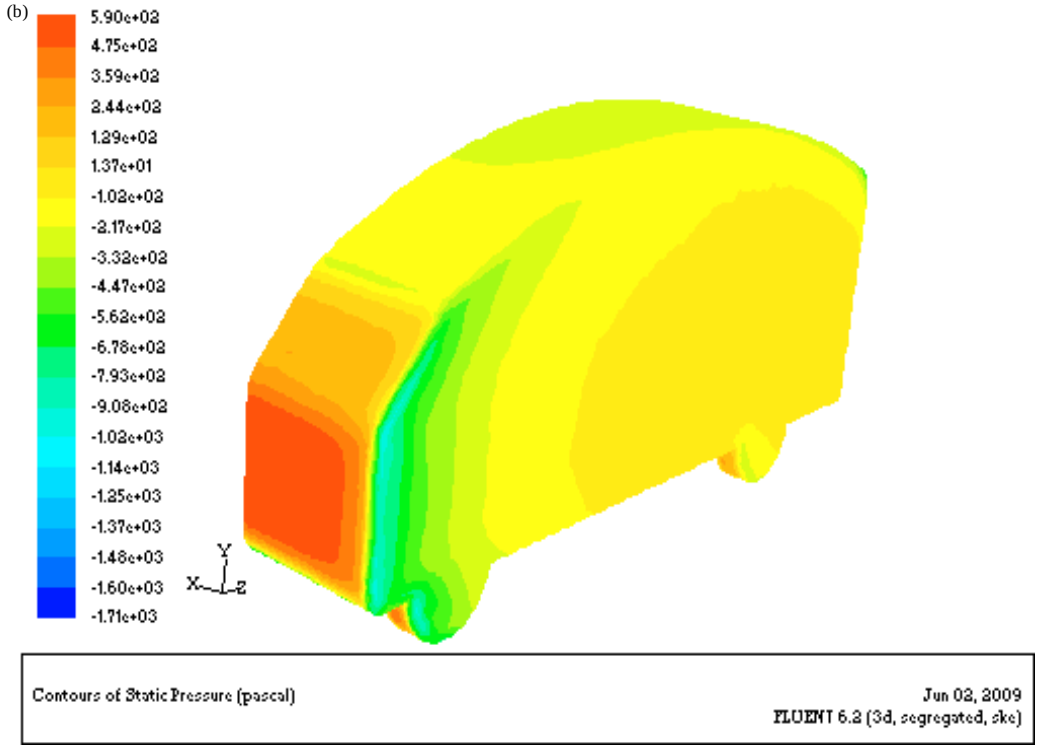

Fig. 17(a-b): Pressure distribution on head surface

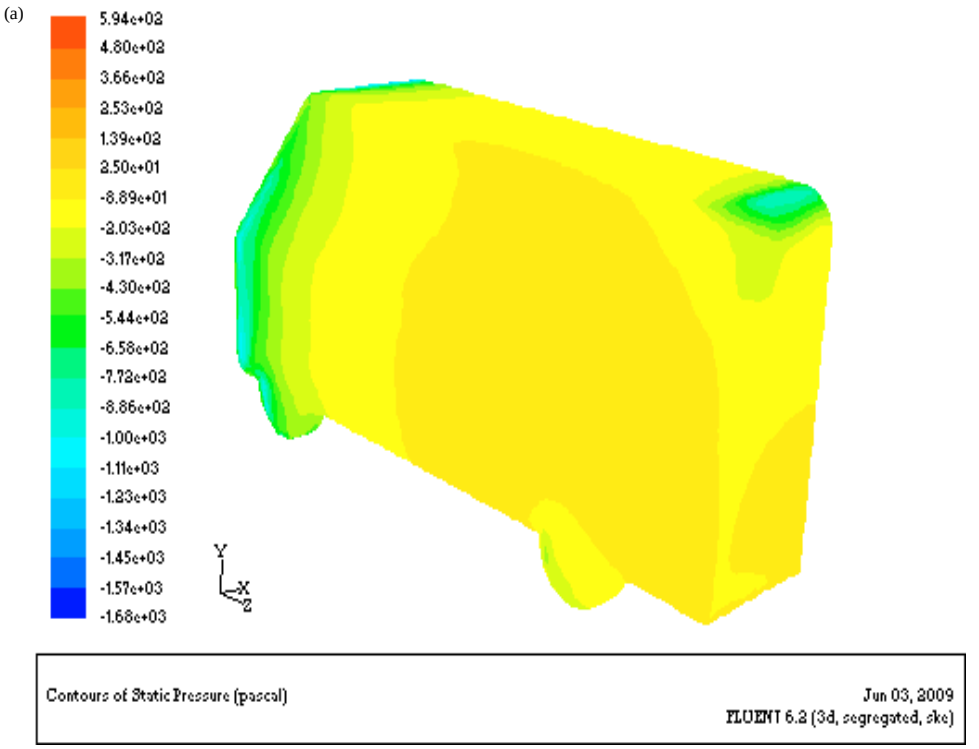

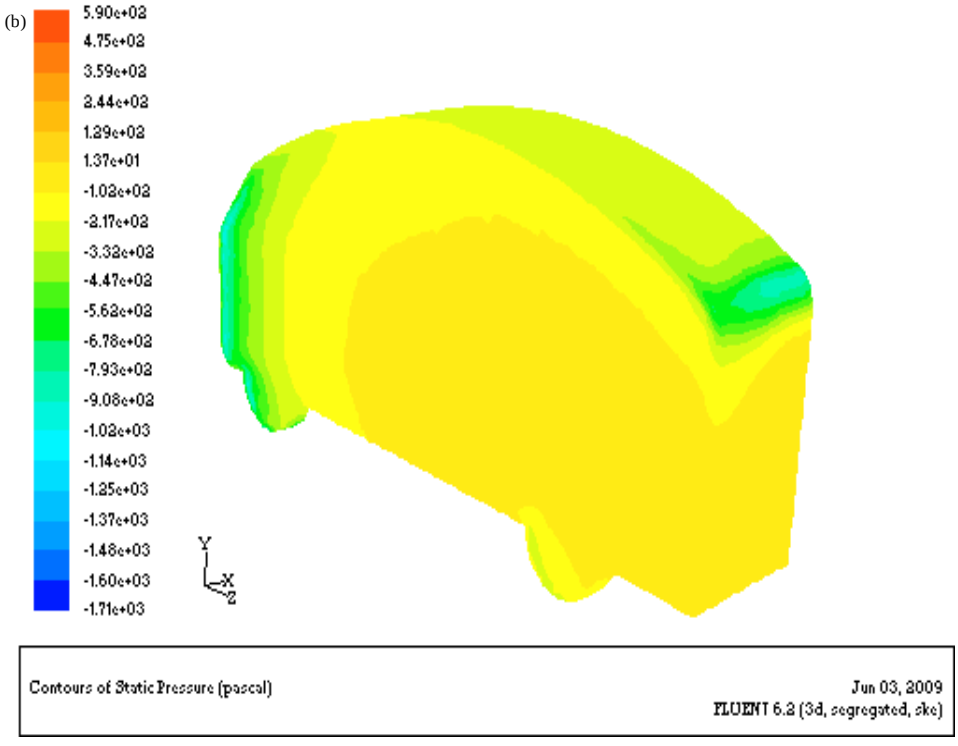

Fig. 18(a-b): Pressure distribution on tail surface

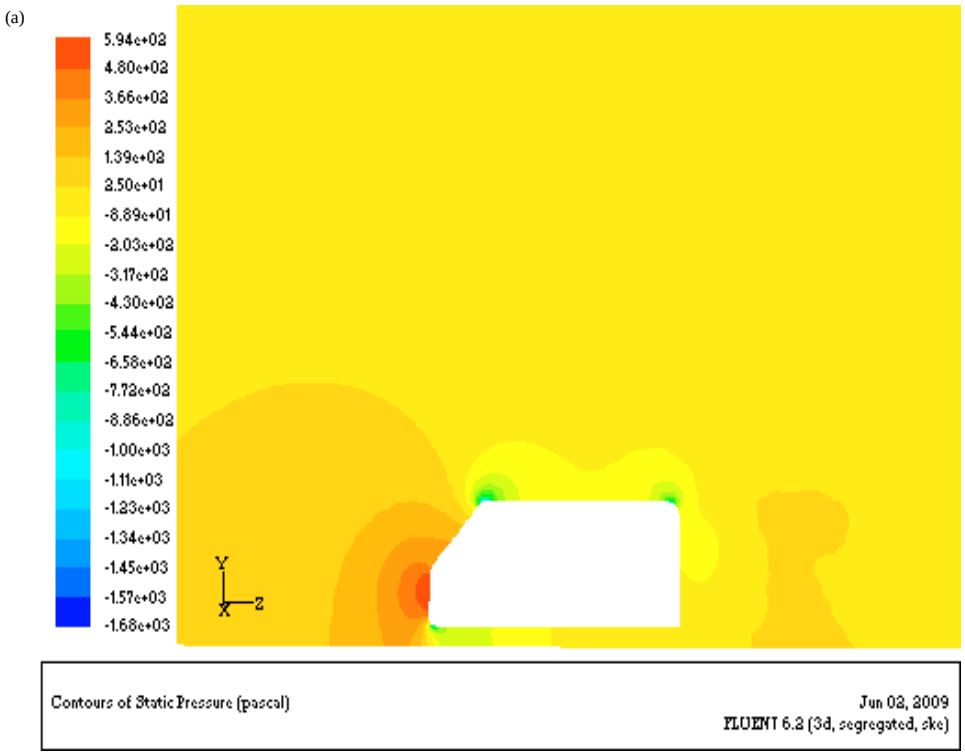

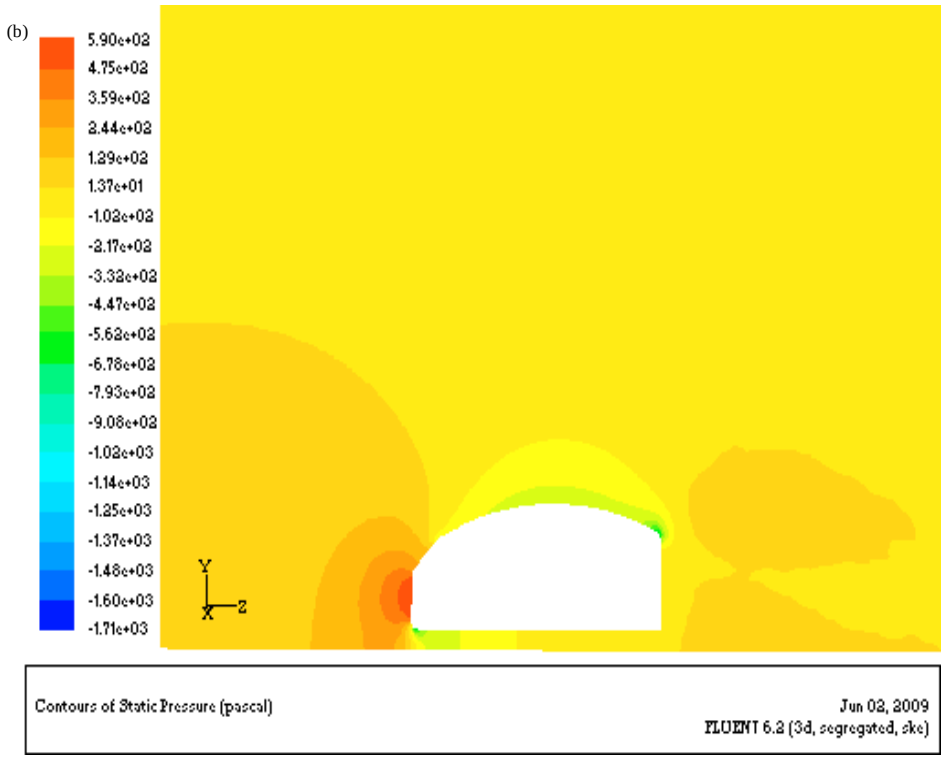

Fig. 19(a-b): Pressure distribution on symmetrical plane

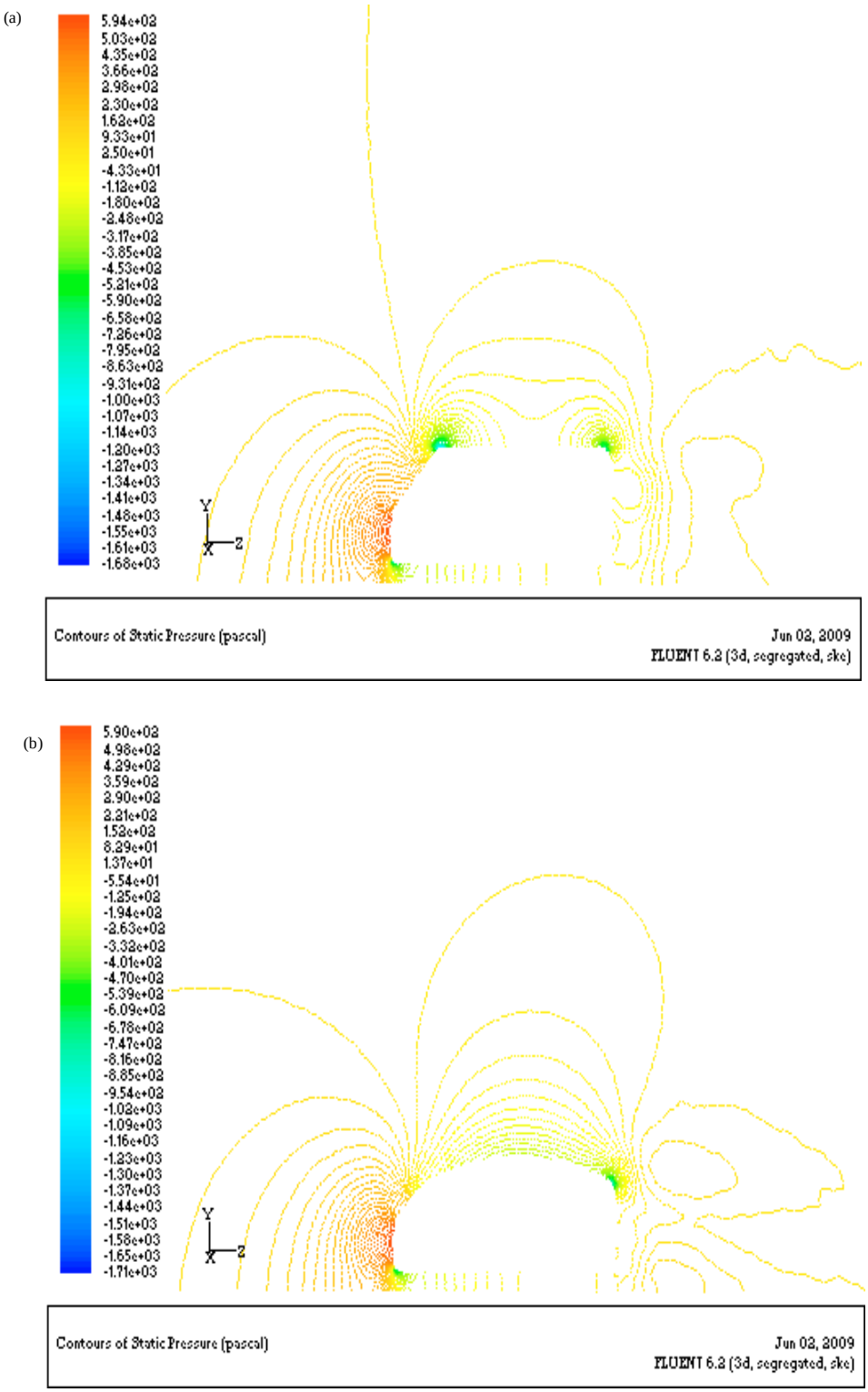

Fig. 20(a-b): Isobar distribution on symmetrical plane

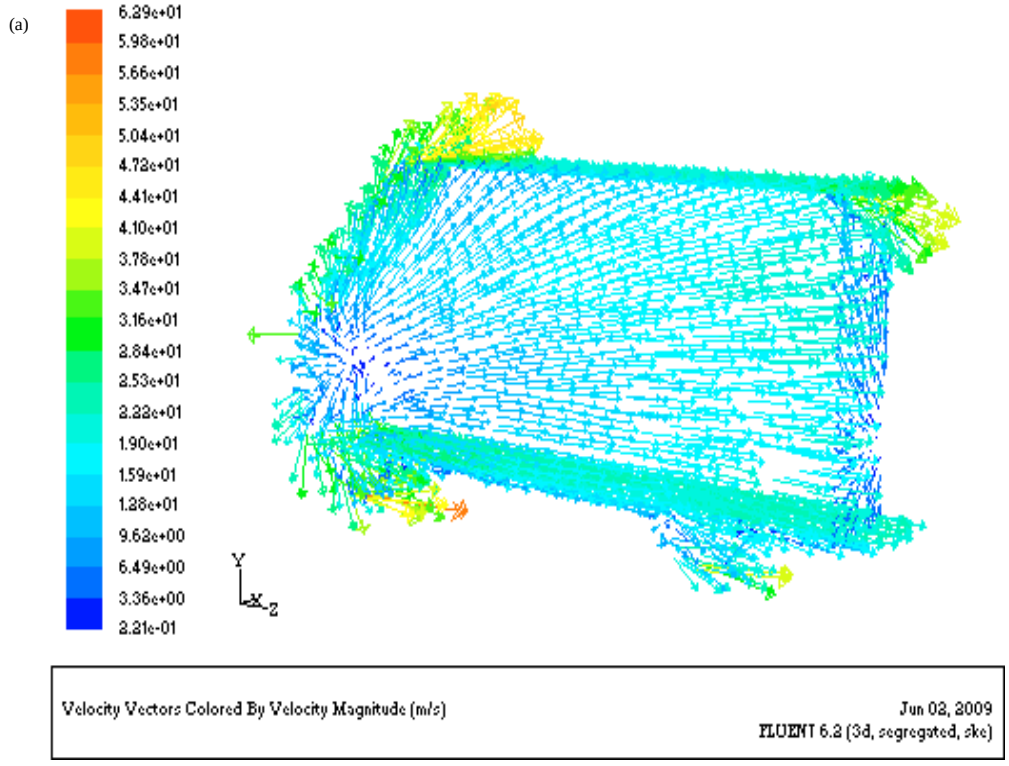

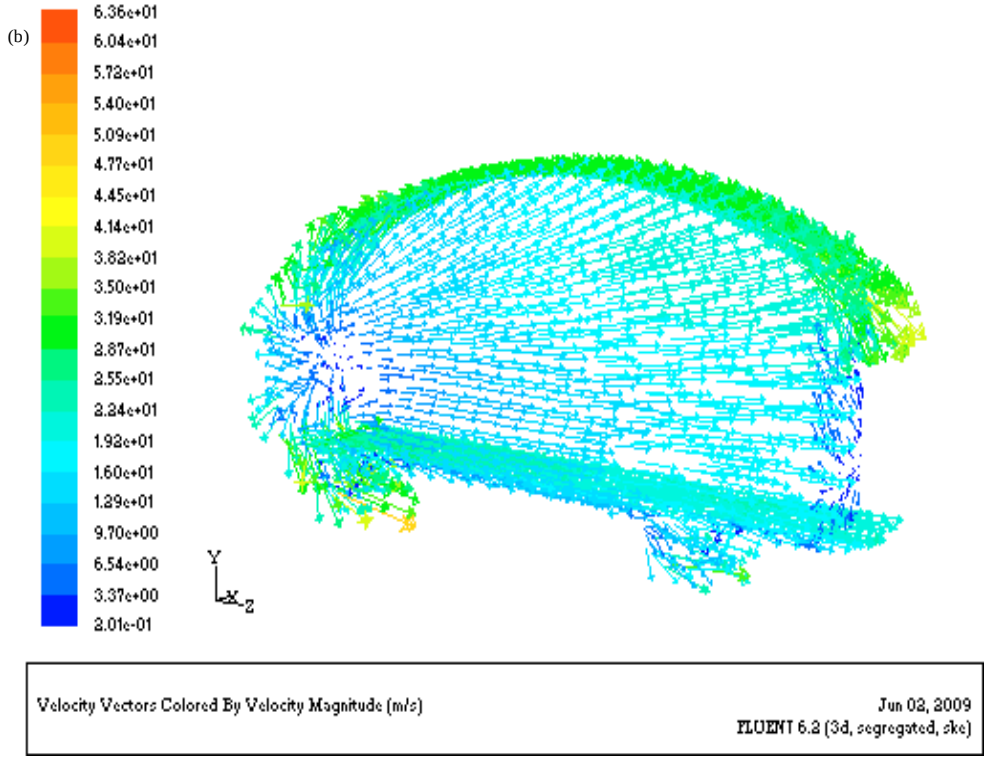

Fig. 21(a-b): Velocity vector on van body surface

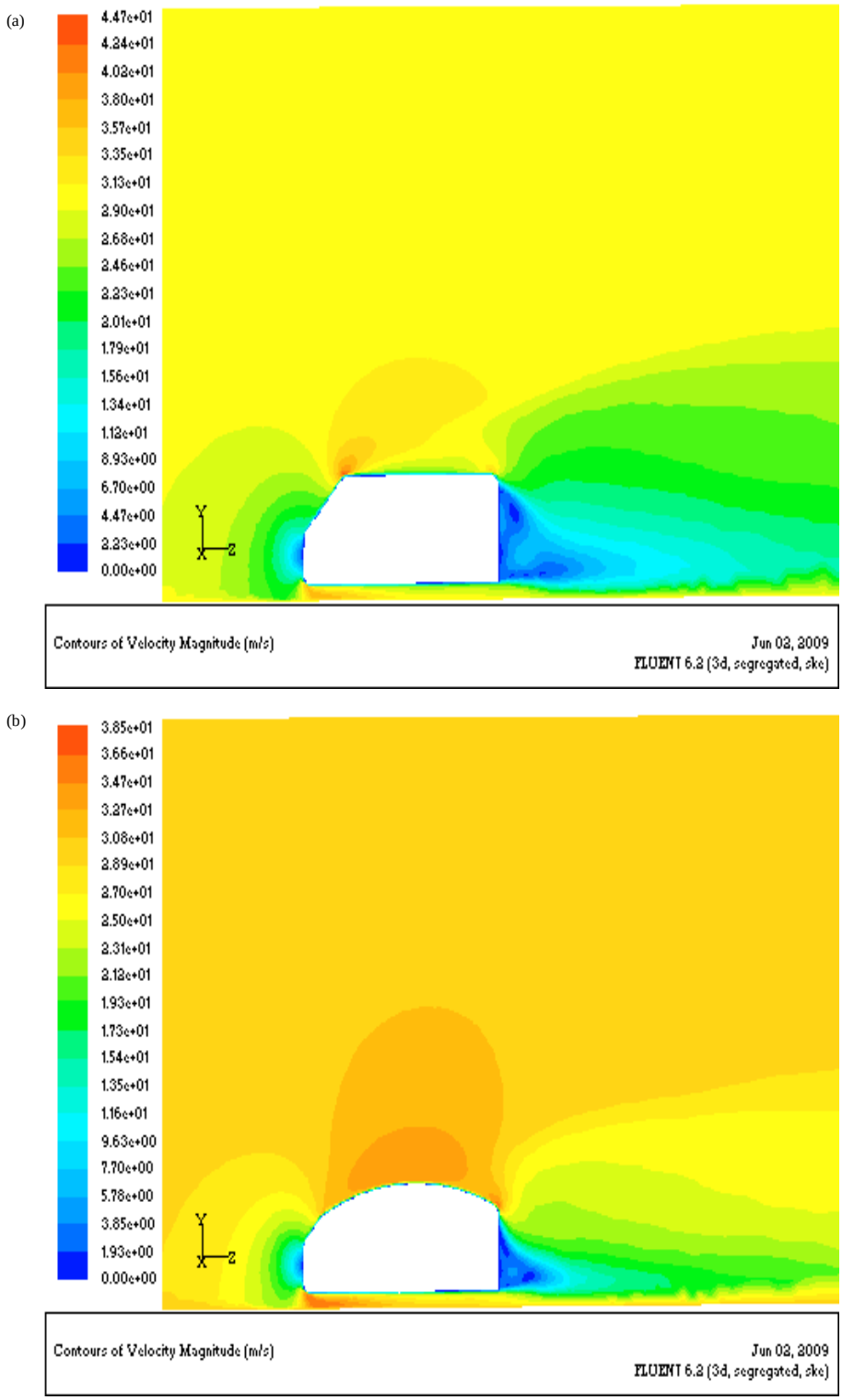

Fig. 22(a-b): Velocity distribution in symmetry plane

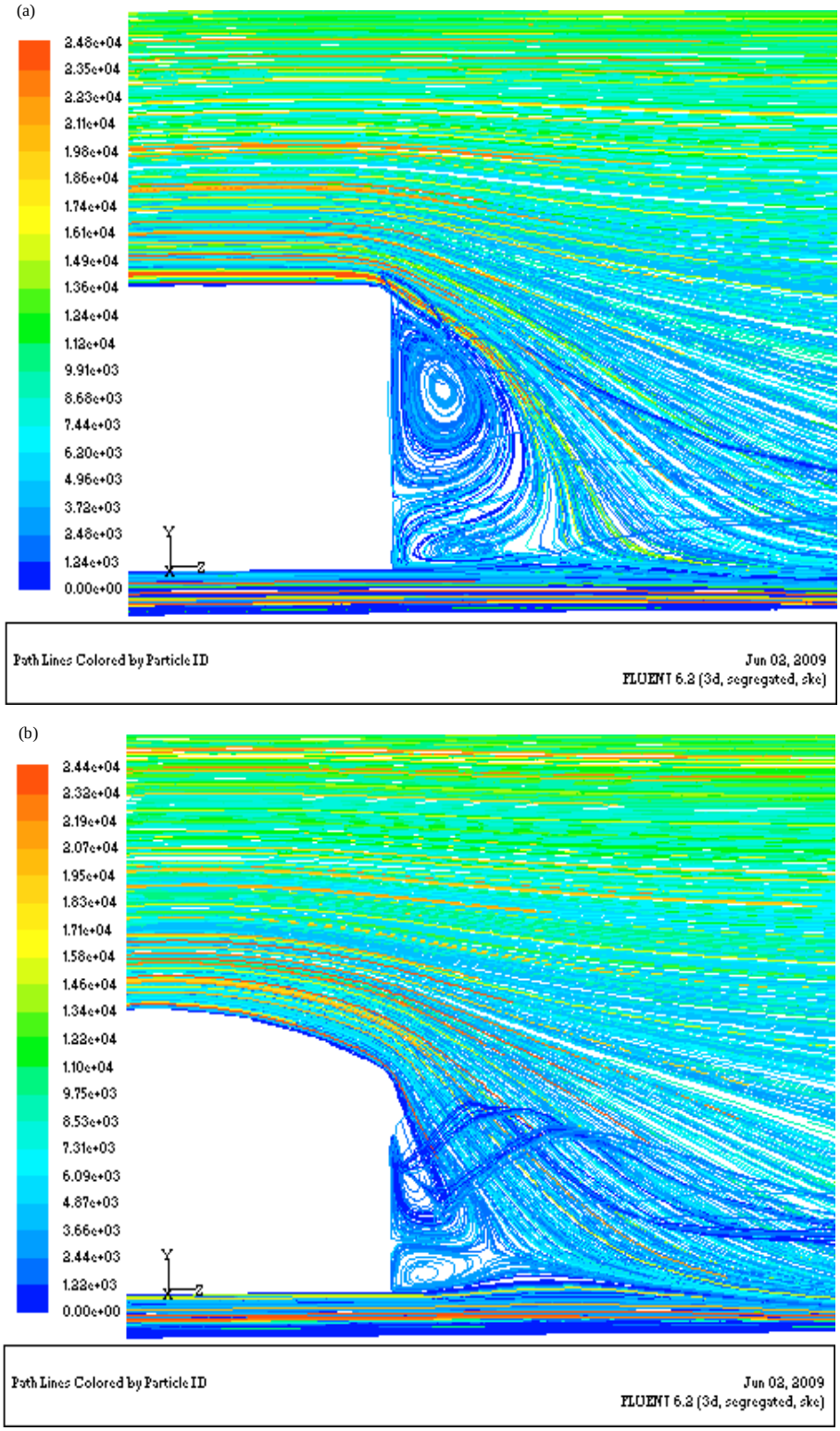

Fig. 23(a-b): Flow chart on symmetry plane

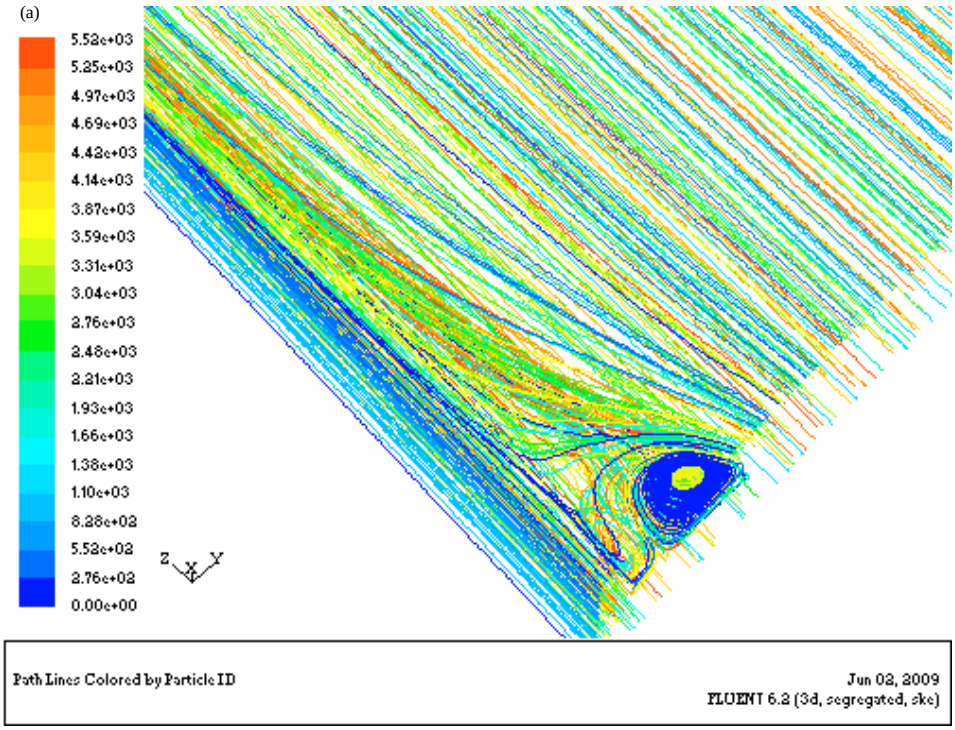

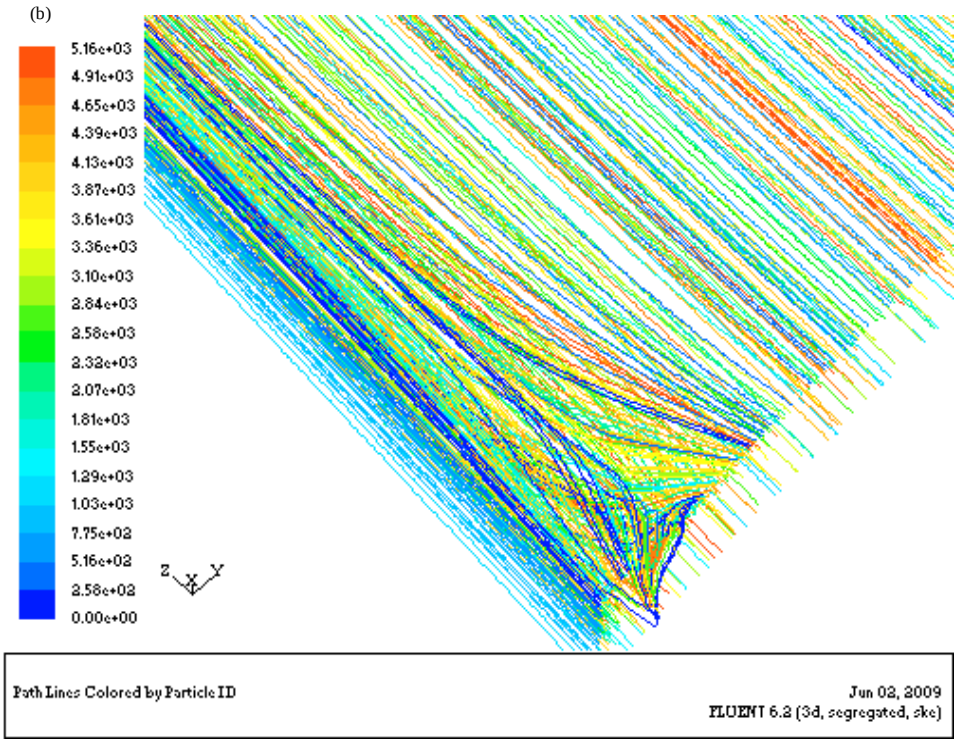

Fig. 24(a-b): Vortex distribution at Z = 230 mm

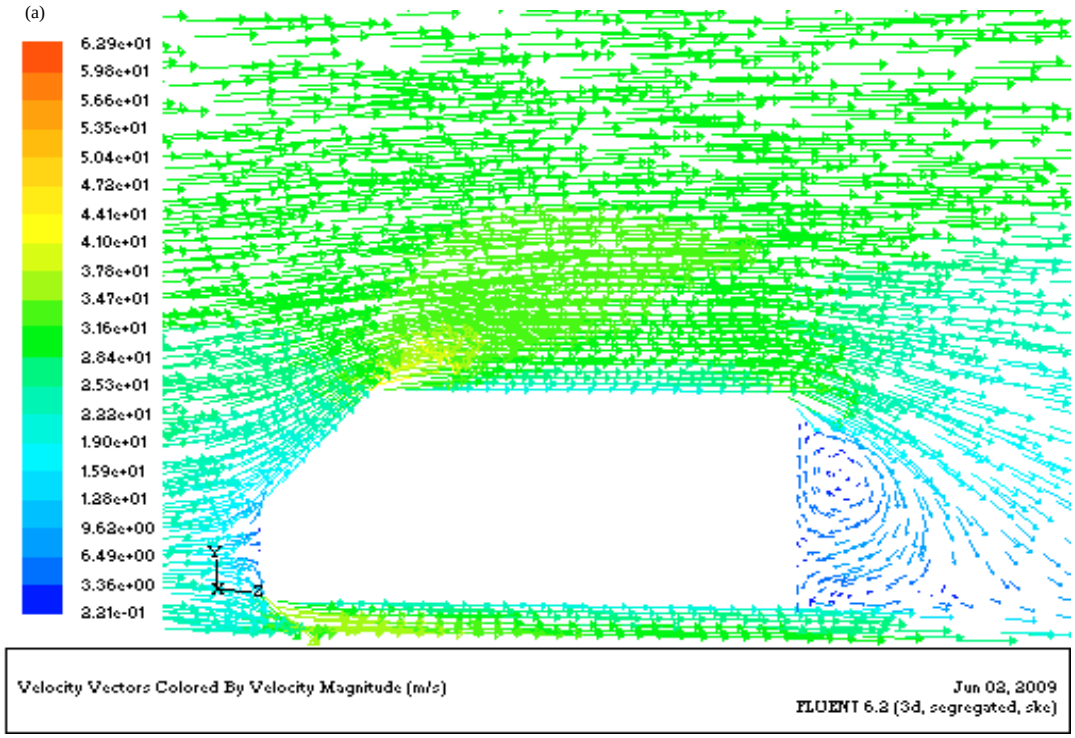

Fig. 25(a-b): Velocity vector in symmetry plane

COMPREHENSIVE ANALYSIS AND CONCLUSION

The objective of this study is to investigate the characteristics of van-induced airflow. The study presents results of numerical investigation, aimed at assessing the effectiveness of the scenario of modified shapes of vans. The Reynolds-averaged Navier-Stokes equations are solved using the finite volume method. The computed distributions of the pressure and the air velocity reveal the effects of four models on the aerodynamic performance. The results show that D-shaped van is a good scenario because of its aerodynamic characteristics being better than those of unimproved model. The geometry and position of the van bodywork and the additive settings should be investigated carefully. If the experimental data or simulation results are absent, the results and analyses in this study can be referred to.

ACKNOWLEDGMENTS

The authors gratefully acknowledge the financial support provided by the Project of National Natural Science Foundation of China (51249001) and Shandong Province Higher Educational Science and Technology Program (J11LD22).

REFERENCES

Al-Garni, A.M. and L.P. Bernal, 2010. Experimental study of a pickup truck near wake. J. Wind Eng. Indus. Aerodyn., 98: 100-112.

Cogotti, A., 2008. Evolution of performance of an automotive wind tunnel. J. Wind Eng. Indus. Aerodyn., 96: 667-700.

Ferrai, P., 2009. The effect of the competition between cars and trucks on the evolution of the motorway transport system. Transp. Res.: Emerging Technol., 17: 558-570.

Gohlke, M., J.F. Beaudoin, M. Amielh and F. Anselmet, 2010. Shape influence on mean forces applied on a ground vehicle under steady cross-wind source. J. Wind Eng. Ind. Aerodyn., 98: 386-391.

Hemida, H. and C. Baker, 2010. Large-eddy simulation of the flow around a freight wagon subjected to a crosswind. Comput. Fluids, 39: 1944-1956.

Huang, Y.D., W. Gao and C.N. Kim, 2010. A numerical study of the train-induced unsteady airflow in a subway tunnel with natural ventilation ducts using the dynamic layering method. J. Hydrodyn. Ser. B, 22: 164-172.

Hyams, D.G., K. Sreenivas, R. Pankajakshan, D.S. Nichols, W.R. Briley and D.L. Whitfield, 2011. Computational simulation of model and full scale class 8 trucks with drag reduction devices. Comput. Fluids, 41: 27-40.

Khaled, M., H. El Hage, F. Harambat and H. Peerhossaini, 2012. Some innovative concepts for car drag reduction: A parametric analysis of aerodynamic forces on a simplified body. J. Wind Eng. Indus. Aerodyn., 107-108: 36-47.

Kieffer, W., S. Moujaes and N. Armbya, 2006. CFD study of section characteristics of formula mazda race car wings. Math. Comput. Modell., 43: 1275-1287.

Kassim, Z.M. and A. Filippone, 2010. Fuel savings on a heavy vehicle via aerodynamic drag reduction. Transp. Res. Part D: Transp. Environ., 15: 275-284.

Li, L., G.S. Du, Z.G. Liu and L. Lei, 2010. The transient aerodynamic characteristics around vans running into a road tunnel. J. Hydrodyn. Ser. B, 22: 283-288.

Nasir, R.E.M., F. Mohamad, R. Kasiran, M.S. Adenan, M.F. Mohamed, M.H. Mat and A.R.A. Ghani, 2012. Aerodynamics of ARTeC's PEC 2011 EMo-C car. Procedia Eng., 41: 1775-1780.

Ni, C.B., R.C. Zhu, G.P. Miao and S.M. Fan, 2010. A method for ship resistance prediction based on CFD computation. Chin. J. Hydrodyn., 25: 579-586.

Rahman, S.M.M. and R. Ikeura, 2012. Optimizing perceived heaviness and motion for lifting objects with a power assist robot system considering change in time constant. Int. J. Smart Sensing Intell. Syst., 5: 458-486.

Regert, T. and T. Lajos, 2007. Description of flow field in the wheelhouses of cars. Int. J. Heat Fluid Flow, 28: 616-629.

Shuk, P., R. Jantz and H.U. Guth, 2012. Oxygen sensor with advanced oxide electrode materials. Int. J. Smart Sensing Intell. Syst., 5: 233-245.

Toshio, K. and K. Kozo, 1992. A review of CFD methods and their application to automobile aerodynamics. SAE Trans., 101: 377-388.

Tsubokura, M., T. Nakashima, M. Kitayama, Y. Ikawa, D.H. Doh and T. Kobayashi, 2010. Large eddy simulation on the unsteady aerodynamic response of a road vehicle in transient crosswinds. Int. J. Heat Fluid Flow, 31: 1075-1086.

Wang, J.B., H. Yu, Y.F. Zhang and R.Q. Cai, 2010. Numerical simulation of viscous wake field and resistance prediction around slow-full ships. Chin. J. Hydrodyn., 25: 648-656.

Watkins, S. and V. Gioacchino, 2008. The effect of vehicle spacing on the aerodynamics of a representative car shape. J. Wind Eng. Ind. Aerodyn., 96: 1232-1239.

Yakhot, V. and S.A. Orszag, 1986. Renormalization group analysis of turbulence. I. Basic theory. J. Scient. Comput., 1: 3-51.

Yao, Y., C.J. Lu, T. Si and K. Zhu, 2010. Experimental investigation on the drag reduction characteristics of traveling wavy wall at high reynolds number in wind tunnel. J. Hydrodyn. Ser. B, 22: 719-724.